T-3766

Phase Equilibrium in the $YO_{1.5}$-BaO-CuO Ternary System

by

Howard Dunn

A thesis submitted to the Faculty and the Board of Trustees of the Colorado School of Mines in partial fulfillment of the requirements for the degree of Master of Science (Metallurgical Engineer).

Golden, Colorado

Date 8-25-89

Signed: Howard Dunn
Howard B. Dunn

Approved: G.L. DePoorter
Dr. G.L. DePoorter
Thesis Advisor

Golden, Colorado

Date 8/25/89

JJ Moore
Dr. John J. Moore
Department Head Metallurgy

ABSTRACT

Review and comparison of existing $YO_{1.5}$-BaO-CuO ternary phase relations revealed several chemical phase equilibrium discrepancies present in this system. Fifteen separate composition mixtures of 99.99% pure CuO, Y_2O_3 and 98.5% pure $Ba(OH)_2 \cdot 8H_2O$ were sintered or melt processed between 700 and 1330 degrees Celsius for .1 to 8 hours, under standard atmospheric conditions to determine ternary phase equilibrium relationships. X-ray diffraction techniques allowed identification of quenched mixture components. The experimental results were utilized to construct a new CuO-$YO_{1.5}$ binary diagram, a new $YO_{1.5}$-BaO-CuO ternary diagram and several psuedo-binary sections depicting previously unconsidered 123, 211, CuO, $YO_{1.5}$ and $BaCuO_2$ equilibrium relations. A new processing technique was developed to produce pure phase incongruent melting compounds from a liquid melt. Pure (less then 2% impurities) 123 orthorhombic "A" type superconducting material with observed meissner effect was produced using this new process technique.

TABLE OF CONTENTS

TABLE OF CONTENTS

TABLE OF CONTENTS

LIST OF FIGURES

(CONTINUED)

LIST OF FIGURES

LIST OF TABLES

Acknowledgements

I would like this opportunity to thank the Colorado Center for Advanced Ceramics for its support and sponsorship of the research program. My thanks to Coors Ceramics Company who provided the essential laboratory equipment to conduct high temperature heating and cooling experiments in addition to the parent compound materials required for this study. I also wish to thank Dr. Gerald DePoorter, my advisor, for his continued availability to discuss problems or results, assist with laboratory equipment acquisition and his approach to providing a high quality educational experience during my stay at CSM. I would also like to extend my gratitude to Dr. John P. Hagar, Dr. Robert Frost, my committee members, and Dr. Readey for their valuable suggestions.

Chapter I

Introduction

High temperature superconductivity discovered in the new yttrium-barium-copper oxide ceramic material has escalated scientific research within the field of ceramic superconducting materials. Tremendous amounts of data have been produced over the last three years since the original discovery of these new ceramic superconductors was made by G. Bednorz and K. Muller (1). Some data, specifically $YO_{1.5}$-BaO-CuO ternary system phase relations, are deficient in completeness and need further investigation and verification to become useful. Research completed at the Colorado Center for Advanced Ceramics provides new information and confirms some data about these $YO_{1.5}$-BaO-CuO ternary system phase relationships. An extensive literature data base compilation of pertinent information associated with the $YO_{1.5}$-BaO-CuO ternary phase diagram and accompanying binary phase diagrams provided several preliminary phase compatibility triangle diagrams and a $YO_{1.5}$-BaO-CuO system liquid phase field relations diagram. Unfortunately correlation between major research literature sources (2, 3, 4, 5, 6, 10) was not unilateral; thus, several binary diagrams exist for each primary binary system associated with the ternary diagram and four separate subsolidus compatibility diagrams were identified for the ternary system at 950 degrees Celsius. A majority of available data and information is confined to phase equilibria at 950 degrees C, because standard $YBa_2Cu_3O_7$ fabrication is completed near this temperature. Liquidus surface phase equilibria data (5,6) in the $YO_{1.5}$-BaO-CuO system is not abundant, and only investigated in detail by T. Asleage and K. Keefer (5). Separate processing methods employed by differing research groups is a probable cause for some discrepancies that appear in the literature work; however, one accurate diagram must be constructed from which additional scientific advancement can proceed. New phase relationships defined from work completed in this study resulted in significant advancement towards accurate $YO_{1.5}$-BaO-CuO ternary system liquidus phase field relations diagram development which is confirmed by comparison with some existing data.

The principle defect in existing research literature is an absence of sufficient equilibrium data verification between one or more research groups. Constructing an accurate and confident phase diagram and extending known equilibria relations in this system from previously undetermined phase relations investigated by this work is the primary research objective. Additional experimental verification and correlation of existing data was completed to substantiate some this work.

Several factors were incorporated to insure the research completed in these investigations accomplished this objective:

1) The new research is partially based on previous scientific work. Most research experimentation was conducted under standard atmospheric conditions similar to previous work. Experimental predicted results were based on equilibria relations defined by earlier works, allowing this work and previous work to be compared. Parent compound chemicals were specified to avoid interferences previously reported by others.

2) Similar scientific guidelines and processing techniques employed by previous investigator's (12) were adopted for the proposed research program; thus, the new data generated builds on a previously existing data base, while providing the opportunity to compare two separate sets of data produced from similar processing techniques.

Chapter II
Existing Phase Relationships in the $YO_{1.5}$-BaO-CuO Ternary System

Introduction:

Existing binary and ternary $YO_{1.5}$-BaO-CuO equilibrium evaluation was important to identify areas of discrepancy and provide general knowledge about current system investigators respective phase compatibility diagrams.

Initially the three primary binary diagrams BaO-CuO, BaO-$YO_{1.5}$, and $YO_{1.5}$-CuO were examined. Several different system diagrams were found to exist for each binary system. This study conducted investigations in the $YO_{1.5}$-CuO system where significant disagreement of eutectic point composition existed between various research groups by 30 mole percent CuO. Comparison of the other proposed binary systems allowed additional modification to the BaO-CuO and BaO-$YO_{1.5}$ diagrams.

Existing ternary compatibility diagrams at 950 C provide four separate subsolidus equilibrium diagrams, One accurate diagram will be constructed to alleviate current discrepancies in these four system diagrams. A single liquidus phase field equilibrium diagram (5) comprises the only detailed information prior to this work regarding ternary liquidus system relations.

Evaluation of these binary diagrams provides insight to possible problems obtaining true equilibrium during experimentation and its sensitivity associated with preparation of 123 superconducting materials with respect to temperature and composition variation. Slight shifts in composition and/or temperature during experimentation could shift an experimental point out of these relatively narrow phase field regions; thus altering true equilibria phase components. Experimental uncertainty and deficiency occurs in both ternary and binary system diagrams. There are approximately twenty-five plus different phase species known or believed to be equilibria phase compounds in the $YO_{1.5}$-BaO-CuO ternary system. Table 1 lists system equilibrium and suspected equilibrium compounds and their respective reference source. Many of these compounds are still questionable equilibria phase components, with some possibly belonging to the $YO_{1.5}$-BaO-CuO-CO_2 quaternary system.

Table 1.

Known or Suspected Equilibrium Components in the $YO_{1.5}$-BaO-CuO Ternary Phase System.

Compound	Binary	Ternary	Reference
BaO (010)	X		2,3,4,5,6,7,10
Ba_2CuO_3 (021)	X		2,4,7,10
$BaCuO_2$ (011)	X		2,3,4,5,6,7
Ba_3CuO_4 (130)	X		2
$Ba_2Cu_2O_2$ (012)	X		10
CuO (001)	X		All
Cu_2O (002)	X		3, this work
$Y_2Cu_2O_5$ (202)	X		All
$YCuO_2$ (101)	X		5,6,10, this work
Y_2O_3 (100)	X		All
Ba_2YO_4 (120)	X		2,3,4,6,10
$Ba_2Y_2O_5$ (220)	X		3,4,6
$Ba_3Y_4O_9$ (430)	X		3,6,10
$Ba_2Y_4O_7$ (420)	X		2,3,4,6
$YBa_3Cu_2O_7$ (123)		X	All
Y_2BaCuO_5 (211)		X	All
$YBa_4Cu_3O_9$ (143)		X	10
$Y_3Ba_8Cu_5O_{18}$ (385)		X	10
$YBa_5Cu_2O_9$ (152)		X	10

Binary System Diagrams:

BaO-CuO. Complete barium-copper-oxide relationships (see figure 1) are still succinctly undefined and more work is needed to determine all existing binary compounds and their respective phase field boundaries. Clarification of equilibrium conditions under which $Ba_2Cu_2O_3$ formation occurs is still required. Figure 1 demonstrates limited phase field relations reported by R.S. Roth et. al. (3). Eutectic composition location, for the reaction BaO + CuO ==> $BaCuO_2$, at 60 mole percent CuO along the BaO-CuO binary is suspect when compared to the CaO-CuO binary sister system, where the $CaCuO_2$ eutectic point occurs at approximately 90 mole percent CuO. Related studies (5) places this eutectic point at approximately 85 mole percent CuO. Identification of Ba_3CuO_4 by K.G. Frase et. al.(2), near the BaO rich end of this Binary is not supported by others (3, 4, 6, 7, 10).

BaO-$YO_{1.5}$. The calculated (3,7) BaO-$YO_{1.5}$ binary, shown in figure 2, clearly shows the possible phase equilibrium relations complexity involved with relative sample mixture temperature and composition variations. This sensitivity makes existing equilibrium compounds difficult to reproduce. Several reported (2, 3, 4, 6, 7) compatible phase compounds near this binary may be present as unequilibrated phase com-

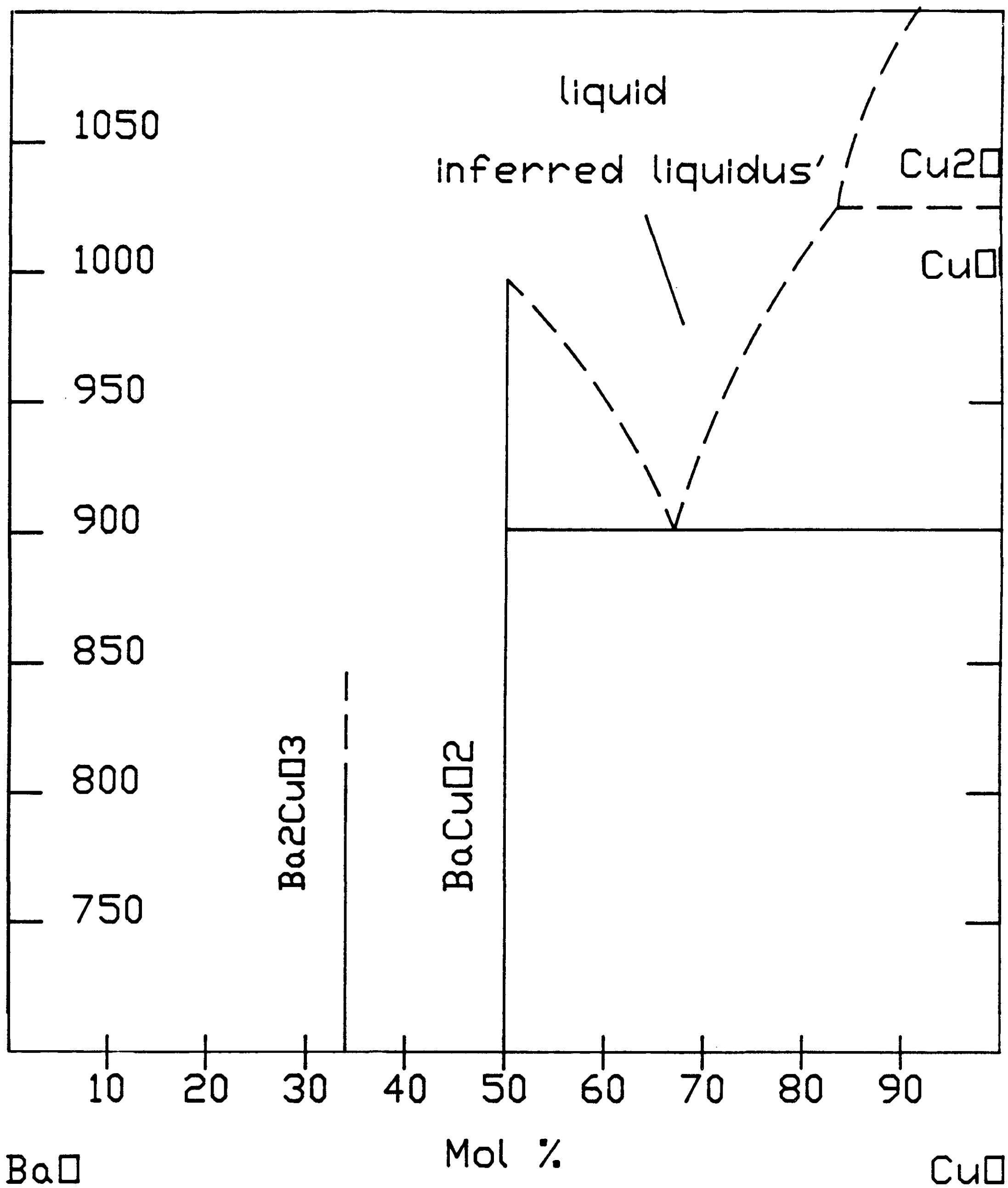

Phase equilibrium model by (3)
for the BaO-CuO binary system.

Figure 1.

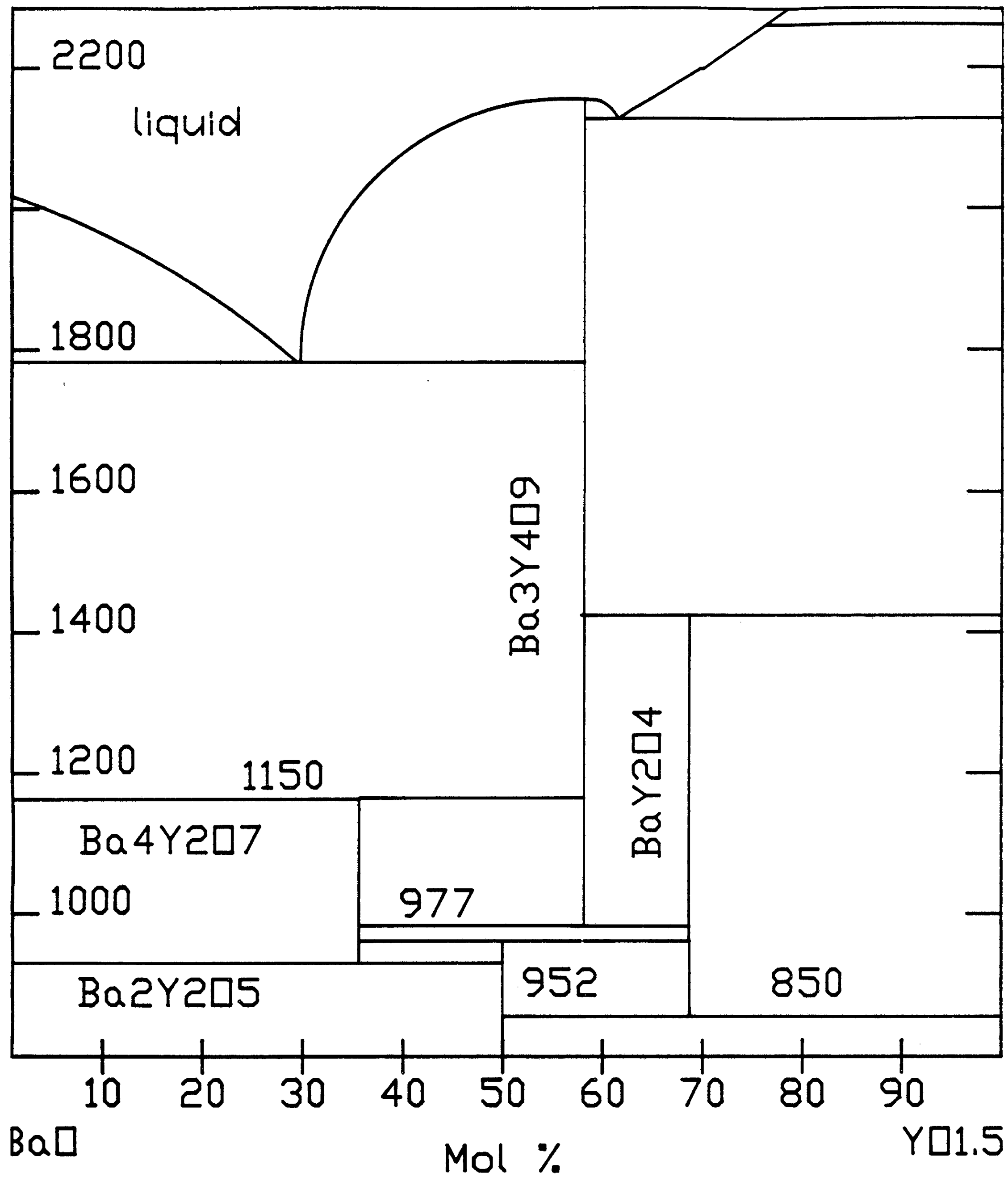

Phase equilibrium model calculated by (3) for the $BaO\text{-}YO_{1.5}$ Binary system.

Figure 2.

ponents. Extrapolation of the binary phase fields into the $YO_{1.5}$-BaO-CuO system demonstrates the difficulty in obtaining true system equilibrium; thus a possible source of discrepancy between actual compatible phases. No low temperature BaO-$YO_{1.5}$ experimental data exists, thus the expected low temperature (below 1200 deg. C) existence of the equilibrium compounds $Ba_2Y_2O_5$ and $Ba_2Y_4O_7$ is based on calculations (3,7) and their reported existence between 900-1000 degrees Celsius by Kwestroo et. al (11). However DeLeeuw et.al. (10) reports these two compounds form only when the barium parent compound is $BaCO_3$ and identified then as oxycarbonates. No binary or ternary equilibria analysis work was conducted at or near this system. Calculated system equilibria (3,7) was not utilized.

$YO_{1.5}$-CuO. This simple binary diagram in figure 3 shows the relatively low melting point of CuO (1230 deg. C), compared to yttrium oxide (greater than 2400 deg. C). A $Y_2Cu_2O_5$ eutectic composition point location discrepancy exists between R.S. Roth et.al. (3,6) and work completed in this study and eutectic composition reported by T. Asleage et. al. (5). A Significant amount of additional research was conducted investigating this binary system to further develop $YO_{1.5}$ -CuO binary phase relations accuracy, with

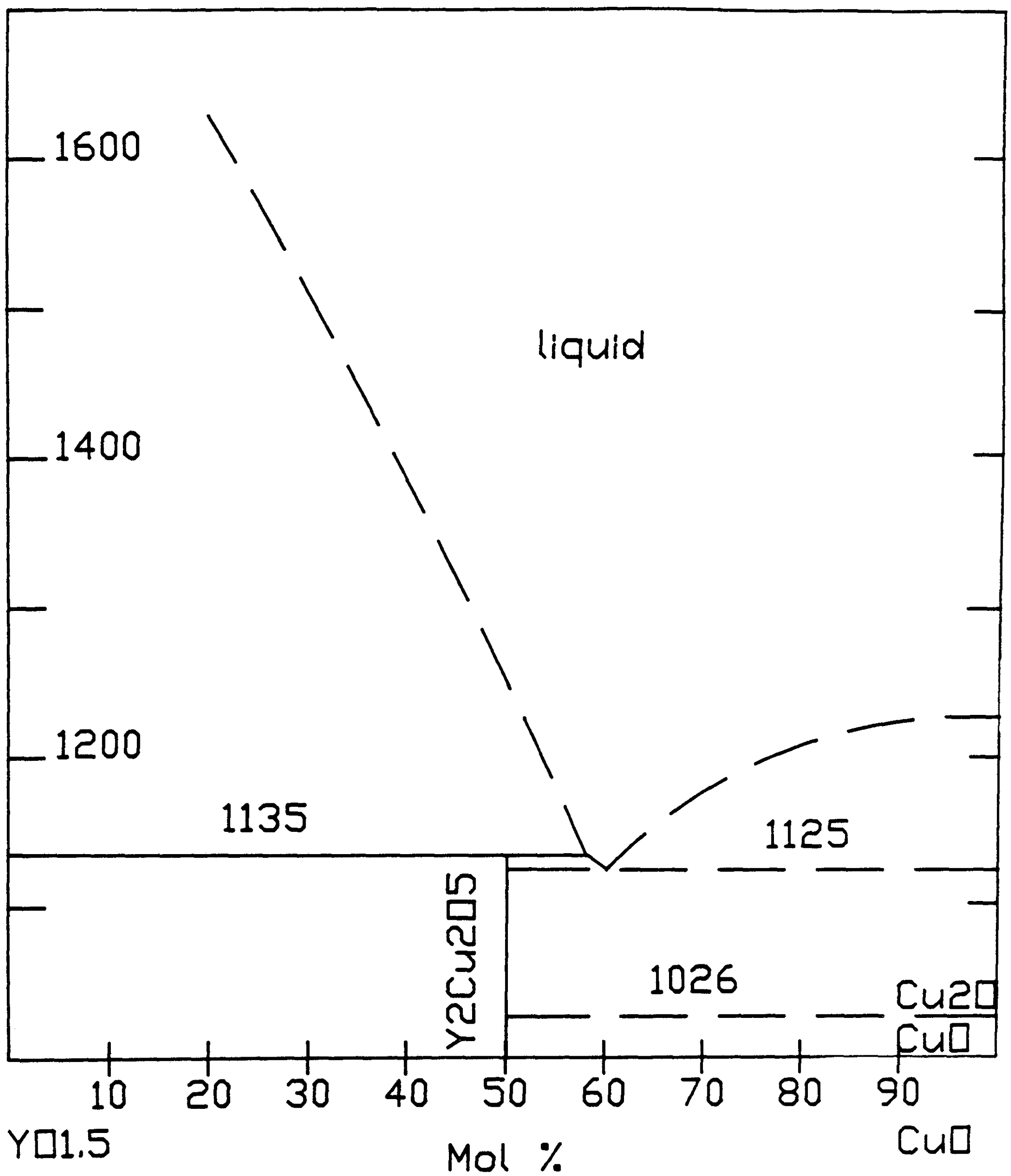

Phase equilibrium model by (3) for the $YO_{1.5}$-CuO Binary system.

Figure 3.

specific attention to $YO_{1.5}$-CuO eutectic composition identification. Figure 3 positions the eutectic point at about 60 mole percent CuO (3).

Ternary Phase compatibilities

Figures 4-7 show phase compatibilities developed by five research groups. Each compatibility diagram defines areas of equilibrated phase components outlined by alkemade lines. Equilibrated phase components are determined by the three compound composition points at each apex of a specific compatibility triangle. If a starting compound mixture, defined by relative parent compound percentages, is located with in the CuO, 123, and $BaCuO_2$ compatibility triangle, then the final subsolidus equilibrated phase components will be CuO, 123, and $BaCuO_2$. Figures 4-7 are equilibrium compatibility isothermal section diagrams at 950 deg. C. Sufficient sample heating and reaction time to allow complete solid state kinetic reaction or precipitation from a liquid melt upon slow mixture cooling to maintain equilibrium status is required to achieve system equilibrium. Mixture quenching from elevated temperatures freezes the reactions at these elevated temperatures, thus allowing investigation of high temperature reactions and equilibrium compositions.

An incongruent melting compound's liquid composition is different from the initial solid compound.

Because the ternary liquidus surface at several points in the diagram is below 950 degrees Celsius these previously designated subsolidus diagrams are indeed representations of liquidus surface compatibilities near the 123 composition point.

Figure 4 phase relations constructed by K.G. Frase and D.R. Clarke agrees with most subsolidus region work completed. The tribarium cuprate compound however, has not been verified by any other research team. The alkemade line from the 132 compound to dibarium cuprate represents a solid solution series between these two compounds because, no end member compound has been found to exist at the copper barium rich end, dashed tie lines were used in this region of the diagram. All authors (2, 3, 4, 5, 10) agree with the 132, 211, and BaY_2O_4 compound compatibilities. The 211 ternary compound exists in equilibrium with seven compounds; including, the 123 superconducting phase, $YO_{1.5}$, $Y_2Cu_2O_5$, CuO, BaY_2O_4, 132, and $BaCuO_2$. The 123 superconducting phase is in equilibrium with only three compounds at this temperature, CuO, $BaCuO_2$ and 211. The 132 compound is the yttrium rich end member to the solid solution series $Ba_{4-y}Y_yCu_2O_x$ and also exists in equilibrium with The 211, $BaCuO_2$,

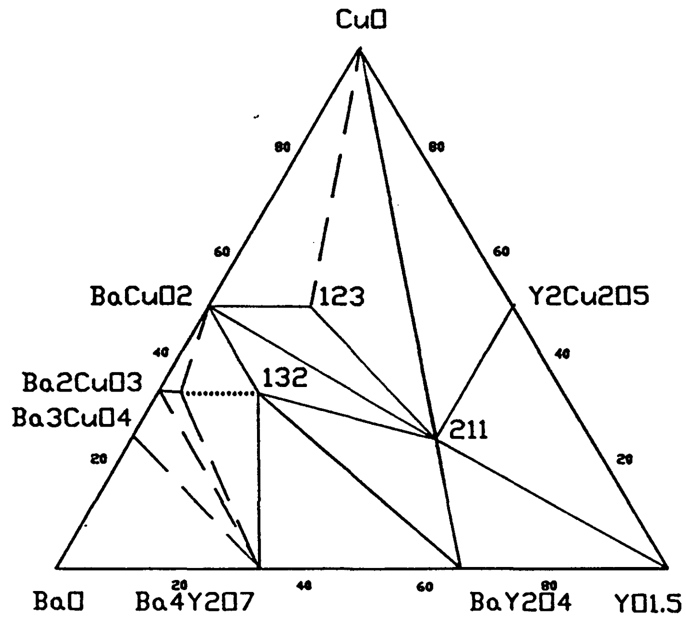

Phase equilibrium model for the $YO_{1.5}$-BaO-CuO system at 950 deg. C. by (2).

Figure 4.

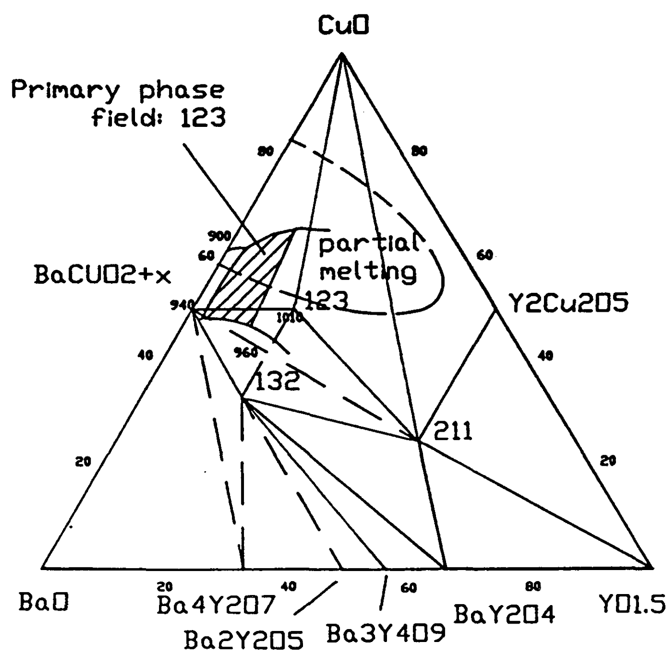

Phase equilibrium model for the $YO_{1.5}$-BaO-CuO system at 950 deg. C. by (4).

Figure 5.

$Ba_4Y_2O_7$, and BaY_2O_4 compounds. The 132 compound and its associated solid solution series component members has recently been reported as oxycarbonate complexes by R.S. Roth et. al.(6).

The phase compatibility diagram in figure 5 completed by R.S. Roth, K.L. Davis, et. al is similar to the diagram completed by K.G. Frase et. al. (2) (figure 4), except in the barium oxide rich corner. In this region R.S. Roth et. al. (3) isolated no equilibrated dibarium or tribarium copper oxide compounds. The dibarium copper oxide compound was fabricated but omission of this compound in their equilibrium diagram indicates the authors (3) believed this compound not to be an equilibrium component in the BaO-CuO binary system. The compatible phases with $BaCuO_2$ are $Ba_4Y_2O_7$, 123, and CuO. Additionally they added $Ba_3Y_4O_9$ to the diagram which, is in equilibrium with $Ba_2Y_2O_5$, 132, and BaY_2O_4. They also report phase compatibility change between $BaCuO_2$, and the 211 compound at about 960 C, above this temperature 123 and 132 are in equilibrium. Variation in temperature and firing times probably cause this crossed tie line discrepancy in the diagram.

G. Wang et. al. (4) in figure 6, closely resembles work completed by K.G. Frase et. al. (1) with one major difference appearing in the BaO rich region of the diagram. They

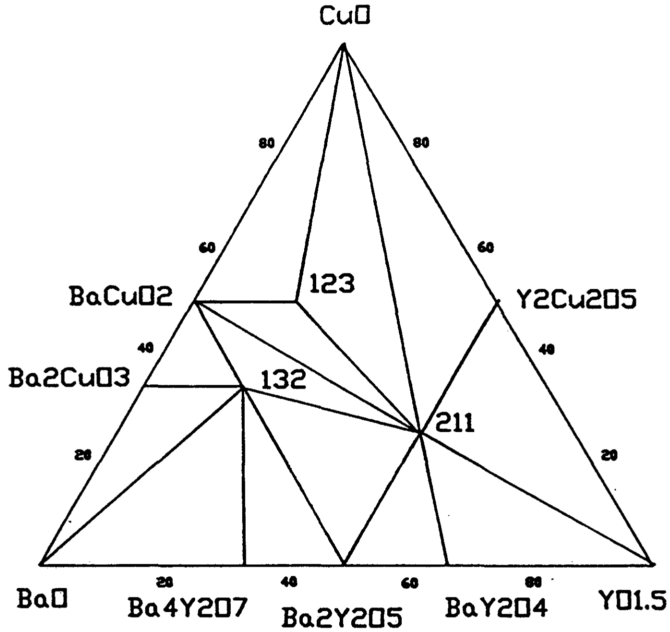

Phase equilibrium model for the $YO_{1.5}$-BaO-CuO system at 950 deg. C. by (3).

Figure 6.

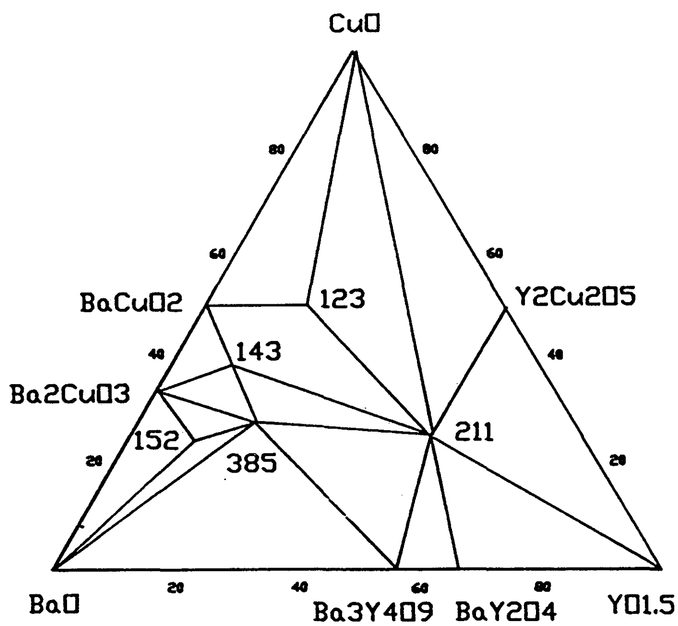

Phase equilibrium model for the $YO_{1.5}$-BaO-CuO system at 950 deg. C. by DeLeeuw et. al. (10).

Figure 7.

(4) identified BaO in all equilibrated ternary compositions in this part of the diagram; thus, the alkemade lines do not equilibrate barium rich yttrium compounds with barium rich copper compounds. The 132 Compound is compatible at this temperature with $BaCuO_2$, $Ba_4Y_2O_7$, and the 211 ternary or green phase compound, after its green color.

DeLeeuw et.al (10), (see figure 7), reports several new ternary compounds (see Table II) which are related to the 132 compound and its solid solution companions. DeLeeuw et. al. state however that some that $Ba_2Y_2O_5$ and $Ba_2Y_4O_7$ were only successfully fabricated in the presents of $BaCO_3$ and thus belong to an oxycarbonate compound system. Additionally new compounds 385 and 438 are reported as modifications to the previously reported 132 disordered perovskite and ordered tetragonal crystal symmetry models. The two new compounds are designated by DeLeeuw et.al. as fitting the tetragonal ordered and orthorhombic ordered symmetry systems respectively.

Liquidus Phase Relationships

Liquidus compatibility phase relations have been investigated in detail (5) and are displayed in figure 8. A majority of the information focuses primarily on phase regions near the 123 phase field. Copper oxide deficient

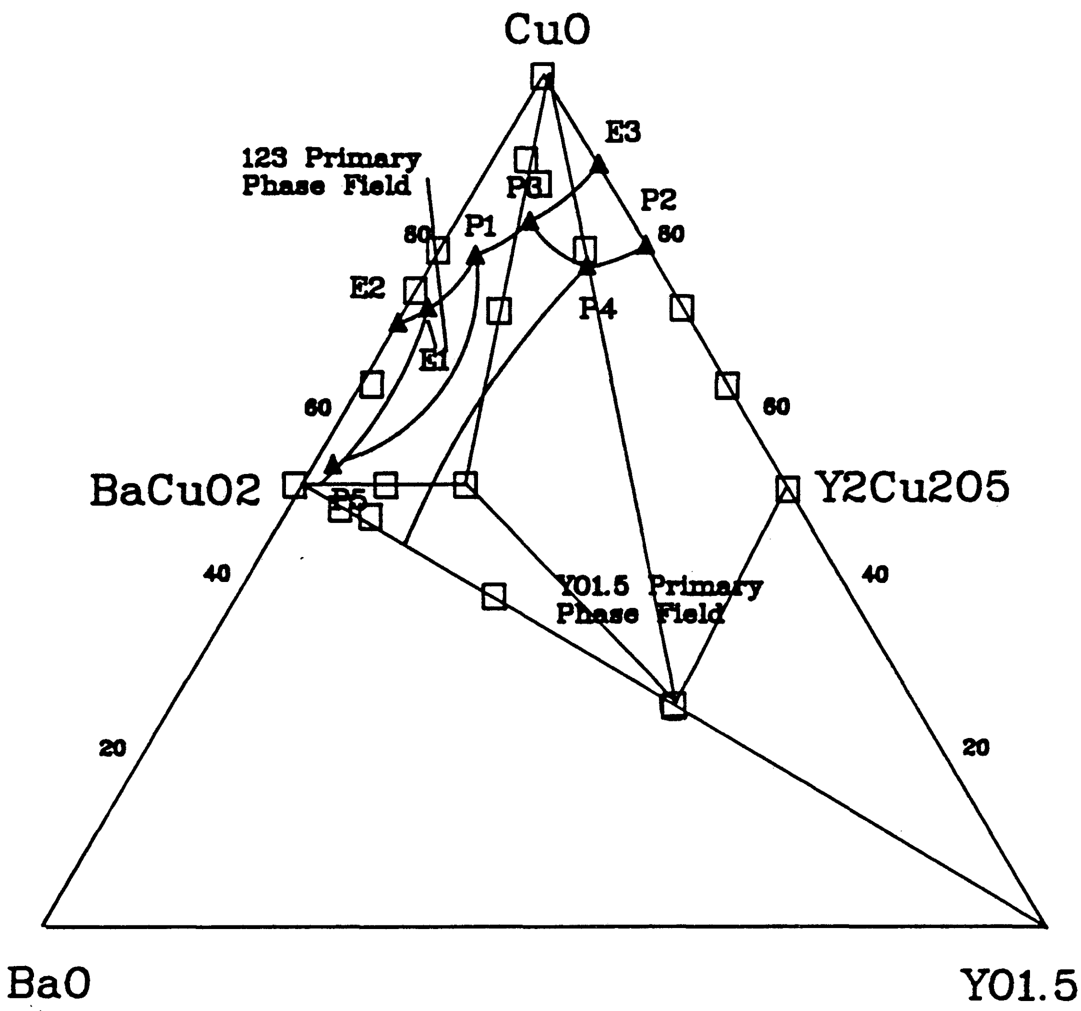

Liquidus phase equilibrium model for the $YO_{1.5}$-BaO-CuO system by (5). Open squares represent locations of experimental compositions (5). Filled triangles locate ternary reaction points. Compatibility triangles are for 950 degrees Celsius.

Figure 8.

regions in the ternary system were not investigated thus equilibrium relationships are omitted in these regions of their diagram. $Ba_3Y_4O_9$ and BaY_2O_4 are the only two inferred stable barium-yttrium compounds in this diagram. The BaO - 132 ternary compound tie line, depicted by G. Wang et. al. (4) at 950 degrees C, is confirmed by DeLeeuw et. al. (10) and might result from the existence of relic BaO because of incomplete system equilibrium; however, because liquidus equilibrium between BaO and 132 offers a simplest compatibility solution for inferred phase field model relations in this region, the new ternary diagram incorporates this tie line. The $BaCuO_2$-211 alkemade line exists below and above subsolidus temperatures. The 132 and 123 alkemade line suggested by (4) is unlikely to exist. This is a very important relationship which still needs further investigation. Ternary reaction points determined by T. Asleage and K. Keefer (5) are displayed in figure 8. A majority of the boundary curve lines, and eutectic and peritectic reaction point locations are inferred and only represent general liquidus phase field relations. Experimental control points by (5), designated by open squares, indicate where additional information will be most useful, what areas are of greater interest, and where further research investigations should be concentrated. Ternary experimental mixture compositions were designed to investigate the following reactions (see fig. 8):

EUTECTIC

E1	123 + $BaCuO_2$ + CuO --> Liquid	890 C
E2	$BaCuO_2$ + CuO --> Liquid	920 C
E3	$Y_2Cu_2O_5$ + Cu_2O --> Liquid	1110 C
E4	211 + $BaCuO_2$ -- > Liquid	1000 C

PERITECTIC

P1	123 + CuO --> 211 + liquid	940 C
P2	$Y_2Cu_2O_5$ + Liquid --> Y_2O_3	1122 C
P3	211 + CuO --> $Y_2Cu_2O_5$ + Liquid	975 C
P4	$Y_2Cu_2O_5$ + 211 --> Y_2O_3 + Liquid	1000 C
P5	123 + $BaCuO_2$ --> 211 + Liquid	1000 C

These are the main reactions that affect component equilibria relations during fabrication of "123" by melt texturing. Reaction chemistries were determined from phase compatibilities of melt textured experimental runs and differential thermal analysis of selected parent compositions.

Conclusions

Comparison of current research data gathered from various publications provided essential information which provided a preliminary understanding of $YO_{1.5}$-BaO-CuO ternary chemical and thermal system liquidus equilibrium conditions. There is enough evidence to substantiate the existence of Ba_2CuO_3; although it is not clear if this compound exists at higher temperatures. K. G. Frase et. al. (2) and G. Wang (4) report that Ba_2CuO_3 is a compatible phase up to 950 C, which is probably a stable subsolidus component in this region. The reporting of CO_2 incorporation into various compounds by (6,10) may be responsible for the discrepancies and difficulties associated with the isolation of specific ternary compounds near and at the 132 composition. Therefore, these alternate or new compounds will not be incorporated into the new equilibrium diagrams as confirmation of these materials by alternate investigators has not been reported. These new compounds may not be true equilibrium components as DeLeeuw et. al. (10) reported difficulty obtaining equilibrated mixtures. These diagrams further assisted research by identifying areas of uncertainty, interest, and providing predictions which enhanced speed of investigations. Standardizing the orientation of the presented diagrams, created by different researchers, has made diagram comparisons much easier.

Chapter III

Experimentation

Introduction

Subsolidus ternary system research investigations often require cooling and heating through eutectic and peritectic reaction points, subsequently preferential melting or precipitation of various compounds occurs; thus care must be used when deciphering equilibrium phase components as relative starting compound parent mixture amounts and their respective heating and cooling paths controls system equilibrium.

Experimental Design

Sintering processes and heating and cooling path configurations were designed to determine new phase relationships and test liquidus equilibrium configurations as shown in figures 4-8. These experimental heating and cooling procedures were partially determined from preliminary experiments that investigated heat soak time requirements to reach stable sample mix equilibrium. Detailed information regarding heating and cooling path design for each experimental run is provided in appendix A.

Five separate mixtures were originally proposed; however fifteen were eventually investigated to assist in locating new phase field boundaries and isolate peritectic and eutectic reaction compositions and temperatures. Table 2 lists the number of experiments conducted with corresponding temperature range, and identified discrepancy or area of interest to be resolved or investigated. Figure 9 shows experimental run compositions and their respective composition locations with in the $YO_{1.5}$-BaO-CuO ternary diagram. Figure 10 outlines a unique ternary diagram area or discrepancy as listed in table 2 that was investigated or resolved by the corresponding experimental runs. Each experiment is associated with a peritectic or eutectic reaction point and was used to isolate these reaction point locations and temperatures i.e. experimental runs 19, and 20 in "area 6" investigated 211 and $YO_{1.5}$ phase field boundary extent and levels of temperature stabilities near the 211 composition point.

These investigations produced both new data which is utilized to construct previously undeveloped phase relationships and accurately define peritectic and eutectic reactions enabling the construction of a new $YO_{1.5}$-BaO-CuO equilibrium diagram.

Initial experimentation determined crucible material types, and sintering and melt processing procedures. Crucible material type selection was based on relative reactivity with the experimental composite mixtures of BaO-CuO and

Table 2.
System features investigated and discrepancies resolved.

Area	Run Numbers	Exper. Temp.	Item of Investigation
1	1,2,3,6,7	25-1075 C	Locate 211 and $YO_{1.5}$ phase field boundary, define 211 phase field, isolate P1 rx temp.
2	4,5,10,11,12, 23,24,39,41	875-1000 C	Define 123 Phase field, isolate E1 and P1 reaction points and temps.
3	13,14,15,16,27	8090-1100 C	Locate $BaCuO_2$-123 phase field boundary, isolate E1 rx temp., define 011 and 123 phase fields.
4	17,18,22,26	930-1200 C	Define 211 phase field area, locate 211-100 boundary, isolate P1 rx temperature.
5	20	1025 C	Verify CuO --> Cu_2O reaction temperature.
6	19,21	1000-1325 C	Produce 211, define upper 211 temp. stability.
7	25	1200 C	Define 100 phase field, determine upper P4 rx limit temperature.
8 & 9	28-38,40	870-1330 C	Define E3 point comp, isolate E3 and P2 rx temps., identify unknown phase component, examine possible O_2 and compound segregation effects on equilibria.
10	8	880 C	Produce $BaCuO_2$(011).

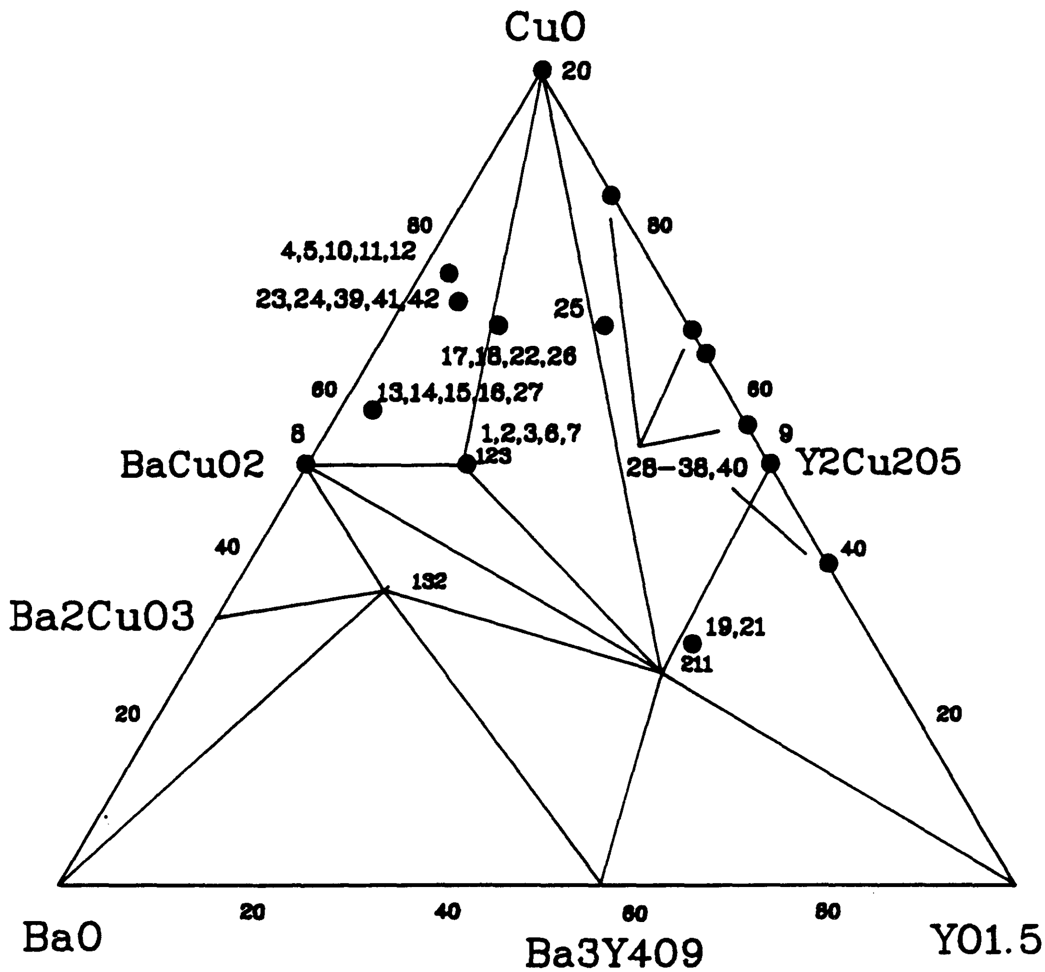

Composition locations of experimental mixtures with corresponding investigation run numbers. Compatibility triangles are for equilibrium relations at 950 deg. C.

Figure 9.

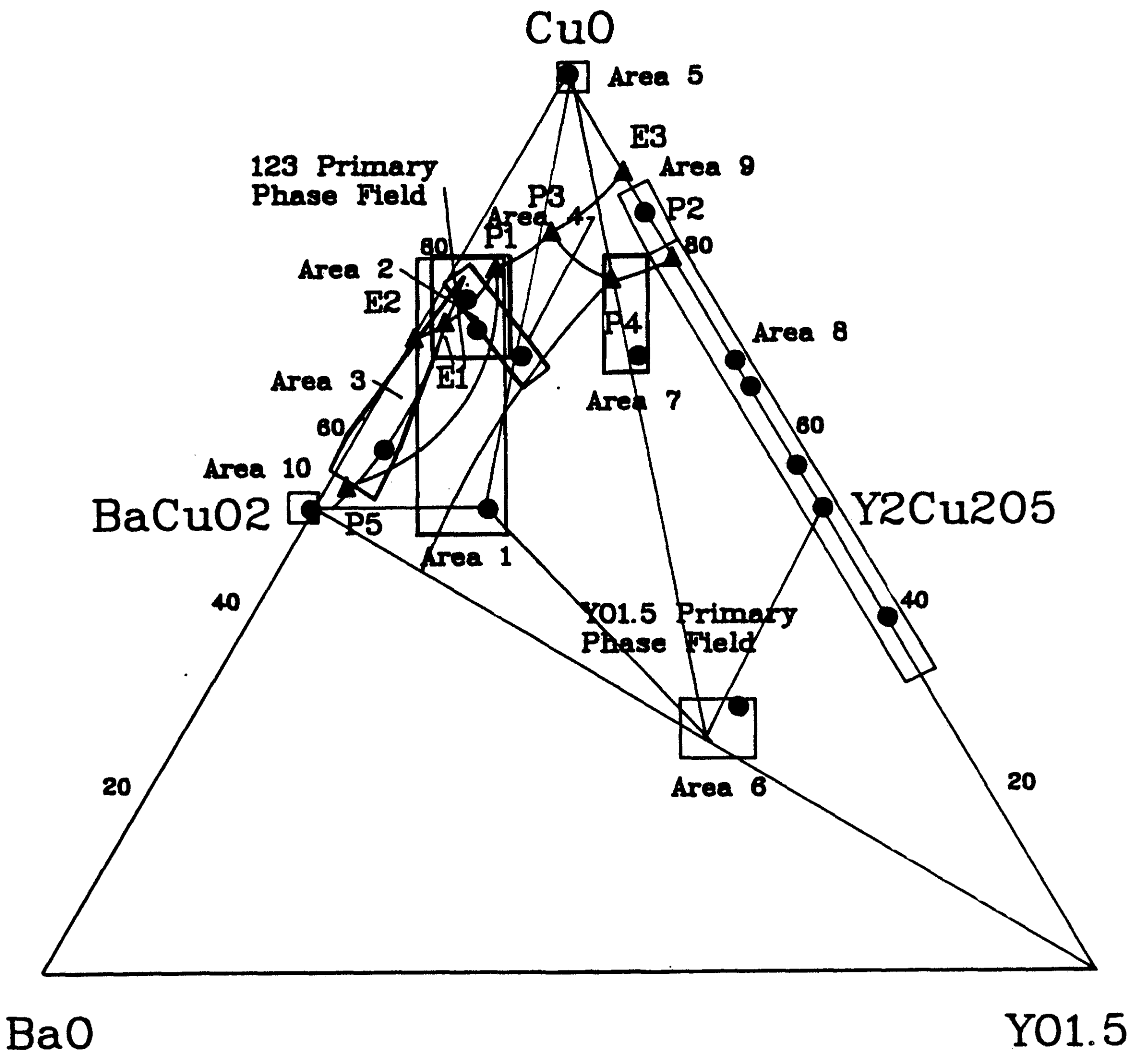

Ternary liquidus phase equilibrium as reported by (5). Filled circles locate this research's experimental composition points. Rectangular outline areas represent areas each enclosed experimental point will help to define equilibria relationships or resolve existing discrepancies as detailed in table 2.

Figure 10.

$YO_{1.5}$. Alumina crucibles were used as minimal reaction occurred with the CuO or BaO enriched sample mixtures.

Experimental Procedure

Several different ratios of CuO, $Ba(OH)_2 \cdot 8H_2O$, and $YO_{1.5}$ powders, provided by Coors Ceramics Company with respective purities (see appendix D) of 99.5%, 99.99%, and 99.99%, were sintered or melt processed at varying temperatures. $BaCO_3$ was not used because of possible oxycarbonate compound formations and reported slow reaction kinetics reported when this parent barium compound was used in previous work (5,6,10). Heating and cooling of the test mixtures was conducted in a small vertical resistance tube furnace modified to allow atmospheric composition control by low pressure chamber flooding. Furnace thermocouple temperature calibration of the to +/- three degrees Celsius was completed by melting a pure gold contact wire and consequently setting the furnace temperature scale to the gold wire melting point by a one point calibration method.

After the desired ratios of yttrium oxide, barium oxide, and copper oxide are mixed by hand grinding in a standard alumina mortar and pestle, the resulting mixture was heated in aluminum oxide crucibles at specified temperatures for a minimum of one hour and up to 15 hours. Equilibrium was achieved after heating for one hour at desired quenching temperature. Several runs with eight hour heat soak times were compared to the phase components in the shorter 1-2 hour runs and no measurable equilibrium difference was observed. It was observed that equilibrium in runs 1-3 was achieved in several minutes when a liquid was present. Subsequent regrinding and heat treating of the varied mixtures was not necessary to remove major contaminants and produce homogeneous products.

Typical techniques were utilized to process the various ceramic powders; however, to analyze high temperature equilibrium phase components at specified temperature levels, most mixtures were quenched to room temperature by rapidly removing the sample from the furnace chamber into room temperature standard atmospheric conditions. Sample cooling rates are estimated to be 300-400 degrees Celsius per minute when initial sample temperature is above 800-900 degrees Celsius. Immediate grinding and x-ray analysis of the sample suppressed hydroscopic material formation by limiting any detectable hydrolysis reactions. There are many variables between various researchers i.e. oxygen furnace atmospheres, mineralizers, carbonated starting compounds, many of which are not completely understood, that may affect reproducibility.

Equilibrium phase relations analysis is closely associated with liquid amounts present at experimental quenching and is discussed in chapter VI. Predicting final experimental mixture equilibrated phase components, using compatibility triangles in the preliminary diagram, has allowed initial diagram configuration comparison with experimental results. Comparison of these predicted phase component result with experimental observations enabled implementation of newly defined phase relations to eliminate discrepancies and produce a ternary equilibrium phase diagram.

Research Investigations

Experimental runs 4, 5, 10, 11, 12 and 23, 24, 39, 41, 42 ("area 2") investigate reaction E1's location and the CuO, and 123 primary phase field boundary locations in the diagram. Runs 1, 2, 3, 6, 7 and 17, 18, 22, 26 study the 211 primary phase field boundaries and the P1 reaction. Additionally runs 1, 2, 3, 6, 7 were used to help construct a psuedo-binary along the 123-211 tie line. Experiments 13, 14, 15, 16, 27 help define $BaCuO_2$ and 123 primary phase field area extent, and verify E1 reaction temperatures. Runs 28-38, and 40 research the $CuO-YO_{1.5}$ binary system phase relationships. Runs 19, and 25 were to check liquidus surface levels and are subsolidus reaction mixtures which never obtained complete equilibrium. Mixtures 8,9, and 20 produced standard compounds used in the x-ray analysis work.

Conclusion

Scanning electron probe evaluation of potential contamination of experimental mixture by reaction with the alumina crucibles, by particles from the alumina mortar and pestle, or impurities in the parent chemicals was investigated. No significant contamination was found to occur. Time and temperature dependance of the experimental mixtures was examined and resulted in reducing soak times dramatically from previously conducted work. Equilibria of a unheated mixture is achieved within minutes upon heating to elevated temperatures if any liquid is present. During sintering equilibrium was achieved fairly rapidly < 1-2 hours near eutectic or peritectic temperatures; however longer soak times tended to allow better crystal formation within the mixture and permit extended sintering of components reducing porosity and grain boundary area. Reaction with crucible walls was consistently observed at elevated temperatures (> 950 C) when starting compounds had relatively high CuO mole percentages, typically greater then 60 percent but, was not significant to warrant attention. Experimental runs were designed to provided the most efficient means of resolving existing phase relations discrepancies. Utilization of the compiled preliminary diagram allows accurate comparison of experimental and existing diagram equilibrium relations and provide a acceptable reference to construct a new diagram based on investigations in this research.

Ternary phase "123" component fabrication is well optimized and standardized. The standard preparation and processing procedure involves desired temperature sintering of the parent compounds copper oxide, barium (hydroxide, or peroxide, carbonate is not used because of its suspected Y-Ba-Cu-CO_2 compound complexes), and yttrium oxide in a non-reactive crucible for eight to twelve hours at desired equilibrium temperature (850-950 deg C), subsequent cooling the sample to room temperature (100 degrees Celsius/hour), grinding to achieve homogeneity, and reheating to with an oxygen atmosphere for an additional eight to twelve hours. The oxygen anneal is optimal, as the 123 compound is highly sensitive to oxygen diffusion into or out of the lattice structure. Small deviations in oxygen content greatly affect the 123 materials' characteristics, including its ability to achieve the superconducting state, its true value T_c, and the crystal symmetry of the final material. The process of reheating or annealing, in an oxygen atmosphere, is employed to optimize orthorhombic 123 "A" (8) formation and is usually required for solid state reaction kinetics.

Chapter IV.
Analytical Techniques

Introduction

Accurate ternary diagram construction depends on accurate equilibrium data collection, and data interpretation. Two types of equilibrium phase data was carefully obtained during experimentation.

1) Experimental mixture equilibrated phase components.

2) Equilibrated quench temperatures and detailed heating and cooling path time-temperature variations. Temperature data was recorded in a lab notebook for future reference and was taken from the preprogrammed digital display on the programmable furnace used for experimental mixture firing and quenching. Individual experiment heating and cooling curves are presented in appendix A. Experimental mixture phase component measurement was achieved by analog analysis of x-ray intensity scans completed for each standard reference and experimental mixture.

Sample Preparation and X-ray Scanning

After mixture quenching, a sample was removed from the crucible and ground to approximately 10 - 50 microns for x-ray diffractometer scanning. Usually less than one hour transpired between grinding and analysis, reducing reaction time for moderately strong hydroscopic material. Each sample was lightly packed in a sample holder and scanned at 40 KV and 25 ma over a two theta distance not less than 45 degrees. Usually from 15 degrees to 75 degrees.

Analog Identification of Mixture components

Unknown mixture intensity peaks were compared to known standard compositions. Overlaying standard peaks onto unknown intensity peaks allowed correlation between known and unknown phase compositions. Once one phase was identified its peaks were labeled and subsequent standard peak comparisons omitted these previously identified peaks (see figure 11.). Standard composition relative intensity data utilized in x-ray pattern analysis is tabulated in appendix B. Originally a program was developed to create standard intensity patterns but, high sensitivity to oxygen positioning and extensive time use developing accurate unit cell models warranted utilization of standard powders for standard intensity pattern development. A majority of these standards were fabricated in the lab and cross-referenced with patterns in literature (5,12). In addition to crystalline phase component identification, approximate relative

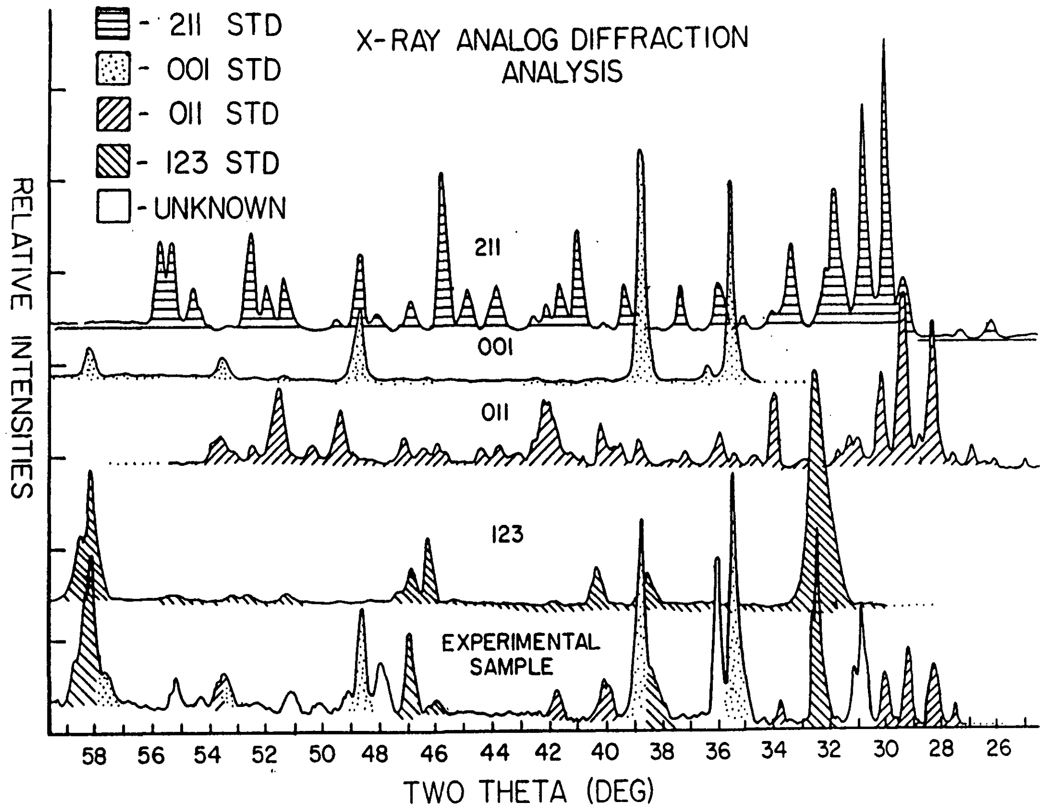

Relative intensity x-ray patterns for reference standards (top four patterns) and unknown experimental mixture (bottom pattern). Analog analysis of the experimental pattern permits comparison of upper standard peak intensities with the unknown pattern to identify the 123, 001, 011 present in the experimental pattern. Note that the 211 pattern dose not match the experimental peaks; thus the phase is absent from this mixture.

Figure 11.

liquid phase percentage amounts present in CuO rich quenched study mixture material could be determined. Percent liquid in CuO enriched (greater than 50 mole %) binary or ternary diagram areas is related to intensity scan background noise amplitude. This phenomena might be explained by the presence of very small CuO grains that form with rapid system cooling. These grains are only slightly larger than initial nucleation points. Copper, which fluoresces strongly under high continuous spectrum radiation near the copper absorption edge, in these grains causes an increase in apparent background noise. As these particles decrease in number or increase in size less fluorescence effect is observed as diffraction increases. This relative correlation between increased background noise and mixture liquid percentage at quenching was consistently observed during investigations that had similar CuO content and quenching processes.

Chapter V.
Primary Binary System
Review and Investigation

Introduction

This chapter will discuss work completed on the primary binary systems BaO-CuO, BaO-$YO_{1.5}$, and $YO_{1.5}$-CuO. The first two system were closely examined and compared with sister systems to check general phase relations. Several areas of suspect configurations were observed. To alleviate these suspect areas all pertinent literature information was reviewed and a best approximation of true equilibrium relations was completed. Experimental investigations were conducted on $YO_{1.5}$-CuO binary system diagram configuration to more accurately define this important binary system.

BaO-CuO Binary System

Figure 12 represents a modification and extension of work completed by R. S. Roth et. al. (3) as presented in figure 1. Extrapolation of the existing sister binary CaO-CuO system onto this binary diagram allows an inferred Ba_2CuO_3 compound melting temperature of 1050 from similar binary compound Ca_2CuO_3 (11) and provides guidelines for Ba_2CuO_2 compound liquidus and solidus lines inference which

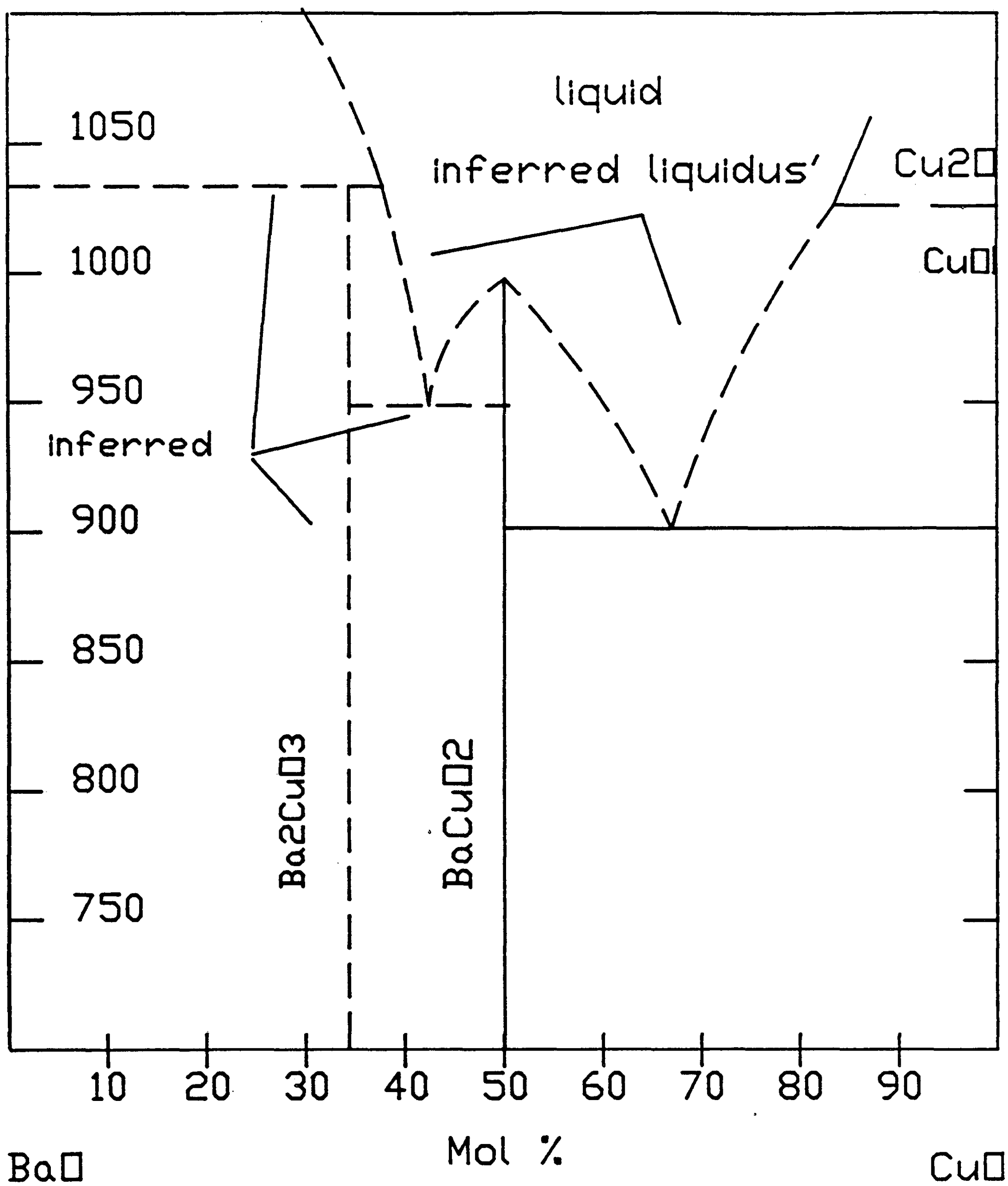

A modified (this work) BaO-CuO binary diagram (3) including interpolation of $BaCu_2O_2$ compatibility from the sister binary BaO-CaO (11).

Figure 12.

were used to generate the Ba_2CuO_3 liquidus and solidus ternary surfaces. However, more information about this intermediate binary compound's liquidus and solidus configuration would greatly enhance ternary liquidus phase field boundaries accuracies.

$BaO-YO_{1.5}$ Binary System

Because $Ba_2Y_2O_5$ and $Ba_2Y_4O_7$ are reported oxycarbonates these two compounds are not incorporated into the binary diagram in figure 13. Comparison of the $BaO-YO_{1.5}$ system with previously investigated sister systems (11) $SrO-Y_2O_3$, $BaO-Dy_2O_3$, and $BaO-La_2O_3$ support the existence of BaY_2O_4 and $Ba_3Y_4O_9$ as stable phase compounds at temperatures in excess of 1200 degrees Celsius and probably are stable to 1000 and 800 degree Celsius respectively. Figure 13 represents the $BaO-YO_{1.5}$ binary diagram (18) with the BaY_2O_4 and $Ba_4Y_4O_9$ compound stabilities extrapolated below 850 deg C, used to construct the ternary phase field relations and compatibilities in the new $YO_{1.5}$-BaO-CuO system diagram.

$YO_{1.5}$ - CuO Binary System

During phase investigation work in CuO rich ternary system areas a discrepancy between existing binary diagrams (figs. 3 & 8) (3, 5, 6), was observed. The discrepancy

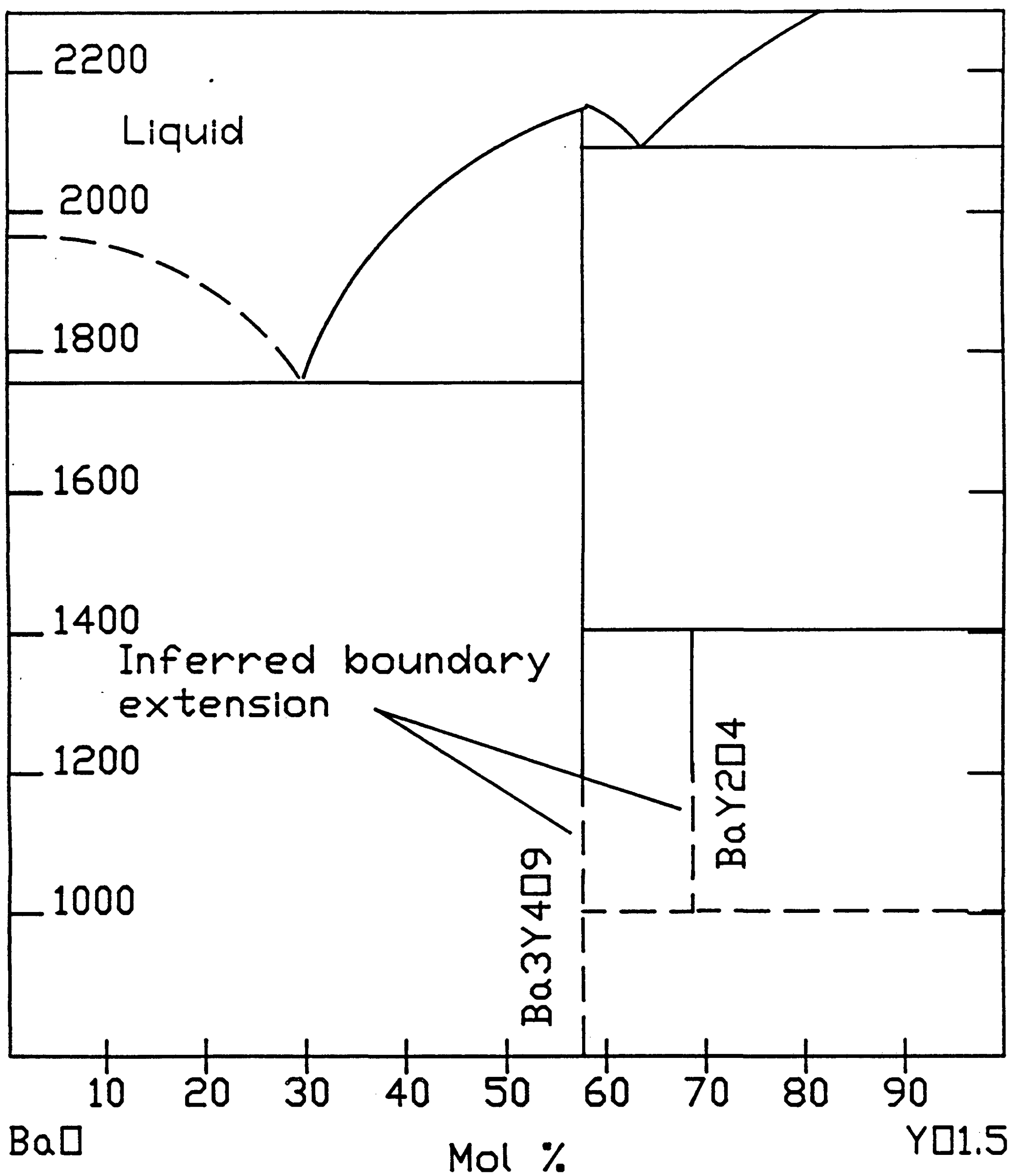

$BaO-YO_{1.5}$ binary modified from (11) to include inferred extension of the $Ba_3Y_4O_9$ and BaY_2O_4 Phase fields to 800 and 1000 deg C. respectively.

Figure 13.

involved binary system eutectic point reaction location between CuO and $YO_{1.5}$. The ternary diagram in figure 8 locates the $Y_2Cu_2O_5$ + CuO ==> Liquid reaction eutectic point at 90 mole percent $YO_{1.5}$ and 1135 degrees Celsius (5,11); however the binary diagram in figure 3 (2) positions this eutectic point at 60 percent $YO_{1.5}$ and 1135 degrees Celsius; thus there is agreement in temperature but not in eutectic point composition.

Eutectic composition. Additional experiments were completed to resolve eutectic composition uncertainty. Thirteen separate experiments (runs 28-38,40) were fired and cooled to define phase and reaction point locations in the binary system. A new binary diagram derived from experiments completed in work is detailed in figure 14. Individual experimental compositions are represented by circles. Approximate composition percent liquid present at quenching is proportional to amount of circle filled.

Liquid percentages were based on observation of sample liquid present at quenching. Excellent agreement between existing data (5) with this studies' data gives a high confidence level in the completed binary diagram accuracy. Variation exists however between this diagram and existing diagrams in addition to the eutectic location. Appearance

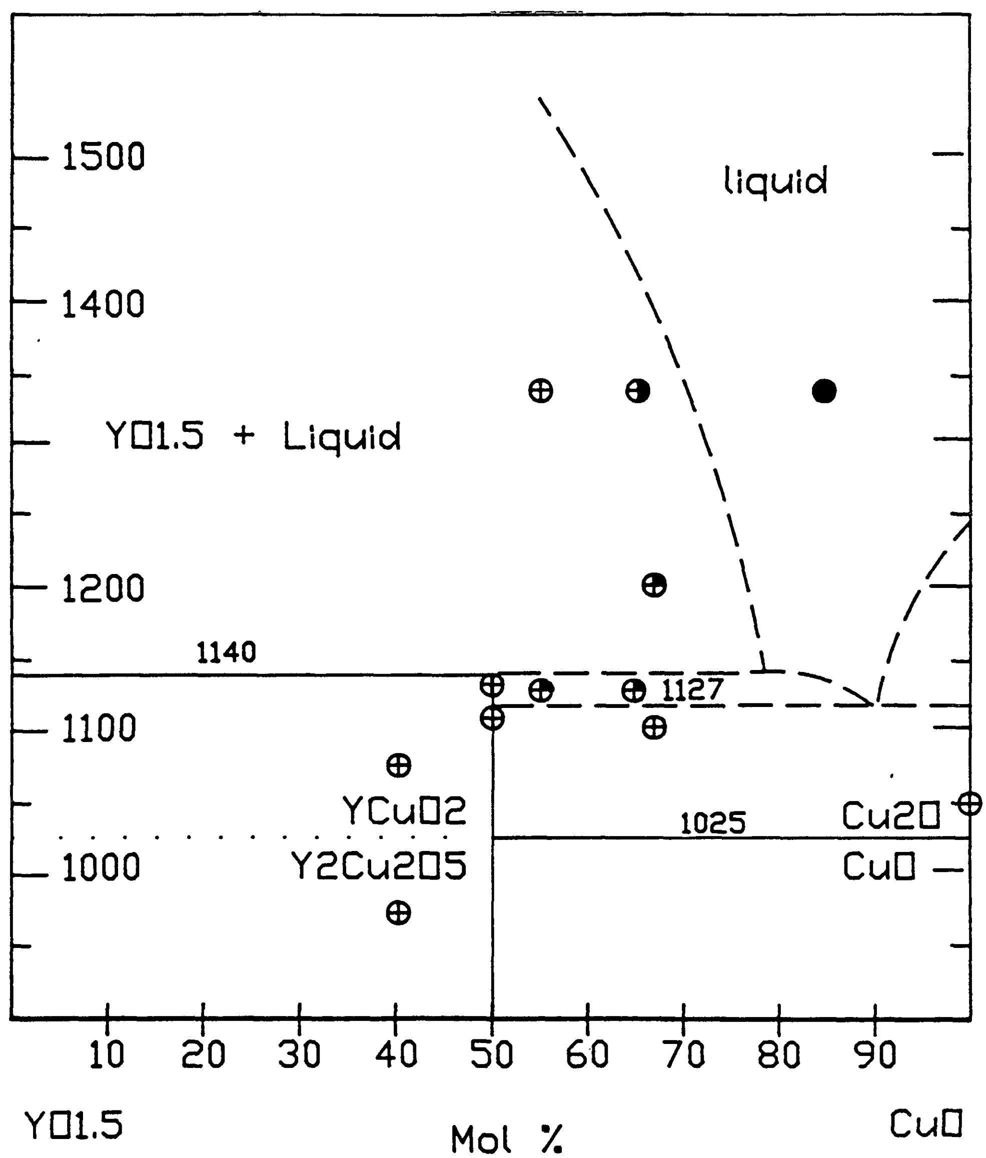

New $YO_{1.5}$-CuO Binary system diagram constructed from investigations by this work. Circles depict experimental control points, with percent liquid present at quenching approximated by percent of circle filled.

Figure 14.

of an additional subsolidus phase, $YCuO_2$, in all experimental mixtures has been observed during these investigations and while also observed by (12,13,17) was not a reported equilibrium component as reported by this work.

Oxygen Potential and the $YCuO_2$ Phase. Problems with matching a standard $Y_2Cu_2O_5$ pattern to a $YO_{1.5}$-CuO binary mixture arose during early research but, was not addressed until this problem again appeared during experimental $YO_{1.5}$ - CuO binary system modeling. Furnace atmosphere control to this point in the investigations was not required, as experimentation was to verify data (2, 3, 4, 5) completed in a standard atmosphere. However, because of complications associated with this unknown standard pattern and based on the assumption that this problem might be connected with furnace atmosphere oxygen potentials, an oxygen purge system was set up. An substantial data base created during investigations to determine the CuO-$YO_{1.5}$ eutectic point composition. This data in all instances showed existence of two separate phases. In addition to standard $Y_2Cu_2O_5$ (12) intensity peaks there also existed, at every composition regardless of quench temperature, and additional unknown phase. Assuming that this phase was dependent on oxygen potential several additional experiments were completed with firing and cooling cycles conducted in a pure O_2 atmosphere. This assumption was supported by the fact that CuO reduces further to Cu_2O at around 1025 degrees Celsius; therefore:

$$Y^{+3} + Cu^{+1} + 2O^{-2} \Longrightarrow YCuO_2 \quad \text{above 1025 deg. C}$$

The selection of $YCuO_2$ as the possible unknown phase was based on reports of this phase occurring in other studies (5,6) and from the above reaction. Verification by SEM composition mapping was not feasible because both phase compositions contain equal percentages of yttrium and copper.

Comparison of $YCuO_2$ relative intensities and $Y_2Cu_2O_5$ peaks indicate that the $YCuO_2$ phase is more predominant at temperatures above 1025 degrees Celsius and lower oxygen potential reaction atmospheres. The determination of different standard intensity peak data was resolved using patterns similar to figures 15 & 16. Because a set of x-ray scan peaks for an individual phase will maintain constant relative intensities with respect to each other, peaks not maintaining a relative constant can be identified and will represent one or more alternate phase compositions present in the experimental mixture. The $Y_2Cu_2O_5$ peaks and $YCuO_2$ peaks are labeled in figures 15 & 16. The Diagram in figure 15 represents an experimental mixture with a higher percentage $Y_2Cu_2O_5$ present compared to $YCuO_2$. Comparing figure 15

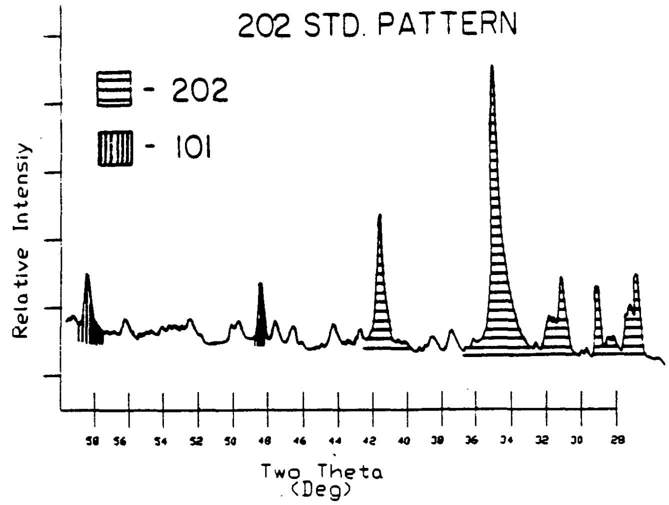

Relative x-ray intensity pattern of $Y_2Cu_2O_5$ and $YCuO_2$ with higher relative percentage of $Y_2Cu_2O_5$ present.

Figure 15.

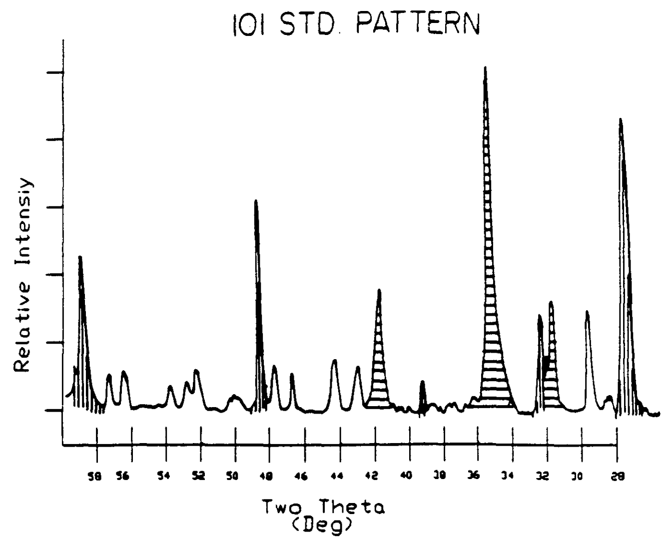

Relative x-ray intensity pattern of $Y_2Cu_2O_5$ and $YCuO_2$ with higher relative percentage of $YCuO_2$ present. These standard reference peaks while, appearing in both patterns, have varying relative intensities with respect to the peaks labelled in fig. 15; thus they represent a unique and different compound, thought to be $YCuO_2$.

Figure 16.

with 16, differentiation between intensity peaks representing $Y_2Cu_2O_5$ and peaks representing $YCuO_2$ occurrence is possible. $YCuO_2$ equilibrium stability and problems with solid-state oxygen diffusion towards the powdered sample center explains existence of both phases in all experimental quenched mixtures. A mixture containing equal amounts of $YO_{1.5}$ and CuO was heated under very low oxygen potential, the crucible was capped to reduce oxygen diffusion into sample, subsequently Cu^{+2} reduction to copper metal was observed in addition to existence of relative high $YCuO_2$ amounts; thus, indicating that greater than standard atmospheric oxygen partial pressure is required to produce pure $Y_2Cu_2O_5$, and that if enough oxygen is not available i.e. standard atmospheric process conditions, the equilibrated intermediate phase composition $YCuO_2$ will be present.

Conclusion

New $YO_{1.5}$ - CuO binary system diagram relationships and acceptable verification of these relationships were established and utilized to construct a new $YO_{1.5}$-CuO binary diagram and assist in new ternary diagram development. Additionally oxygen potential dependence of binary system phase species was investigated and determined to only slightly affect equilibrate phase components at any one specified temperature and compositional point. $YCuO_2$ compound formation under moderate to low oxygen potentials during processing in this binary system suggests similar ternary system problems may occur.

Chapter VI.
$YO_{1.5}$-BaO-CuO Ternary Phase Equilibrium Diagram

Introduction

Copper enriched $YO_{1.5}$-BaO-CuO ternary liquid phase chemical equilibrium relationships were determined and a new $YO_{1.5}$-BaO-CuO ternary diagram was completed. Previous data (5) generally supports these newly defined phase field relationships, peritectic, and eutectic reaction temperatures. The equilibrium compatibilities and reaction chemistries determined by T. Asleage and K. Keefer (5) compliment this work and were subsequently partially utilized to verify or assist $YO_{1.5}$-BaO-CuO diagram construction. The new ternary diagram is depicted in figure 17. Phase field boundary areas and equilibria compatibilities determined in this research are confirmed by some original diagram relations, from previous works. Higher confidence in 123 and 211, 011, 001, and 202 compatibilities have been established over previous diagrams. This study completely identifies the 123 liquidus phase area and reactions with ternary composition mixtures having greater than 50 mole percent CuO. Partial melting in the CuO rich end of the ternary at 950 C (3) system shows some agreement with current liquidus surface modeling (5,

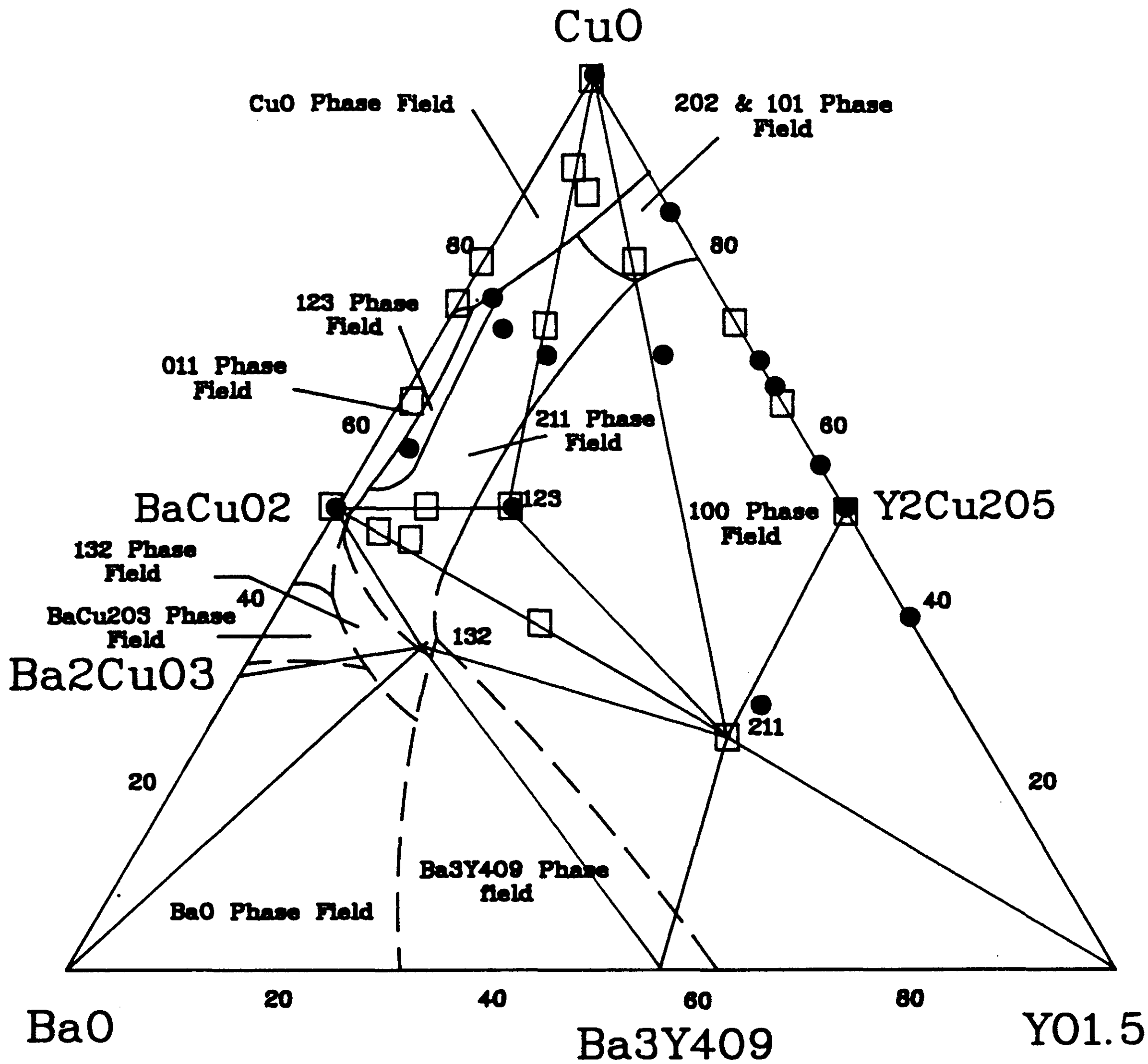

New liquidus phase equilibrium diagram for the $YO_{1.5}$-BaO-CuO ternary system displaying the new 123 primary phase field area extent. The phase field locations in the copper oxide deficient regions of the system are inferred (dashed lines). Filled circles represent experimental compositional control by this research. Open squares identify experimental compositions by (5). Alkemade lines depict compatibilities at 950 deg. C. The 132 phase field is shown equilibrated with BaO; however the Ba_2CuO_3 phase field could connect with $Ba_3Y_4O_5$ liquidus region to eliminate this compatibility.

Figure 17.

This work), as partial melting would be expected to occur in this region of the system. Ternary reaction points locations require further investigation; however, copper rich (CuO greater than 50 mole %) compatibility triangles and system eutectic and peritectic reaction temperatures have been well defined. Earlier work (2,3,4) was used to approximate the 132 phase field boundary and to locate possible 132, and intermediate barium-yttrium and barium-copper compound phase compatibilities. The 132 and associated barium rich yttria compounds, both reported oxycarbonates (6,10) are new system discrepancies.

Phase component numbers and the phase rule

Several mixtures had more than four phase components present violating the phase rule when mixtures are not eutectic or peritectic reaction points. The possible number of phases present is defined by the phase rule:

$$F + P = C + 1;$$

where pressure and vapor phase components are fixed and F is system degrees of freedom at any designated point, P is phase numbers present at any specified point in the system, and C is system parent components numbers i.e. $YO_{1.5}$, BaO, and CuO for this ternary diagram. During normal sample cooling or heating two degrees of freedom exist in a ternary system. System temperature variance during mixture cooling or heating and system compositional change during component precipitation or melting upon system cooling or heating respectively comprise these two degrees of freedom. The possible number of phases present at any point in time, not at a reaction point, from the phase rule, must be less then or equal to three.

Ternary Eutectic and Peritectic Reactions

Figure 18 correlates experimental compositions and run numbers with distinct peritectic, eutectic, or liquidus phase field equilibria each separate mixture defines. The seven reactions depicted in figure 18 represent newly determined reaction chemistries and temperatures or verify previously reported reactions (5). Runs 1-27 were specifically designed to isolate peritectic and eutectic reaction temperatures while investigating related cooling path reactions along phase boundary curves.

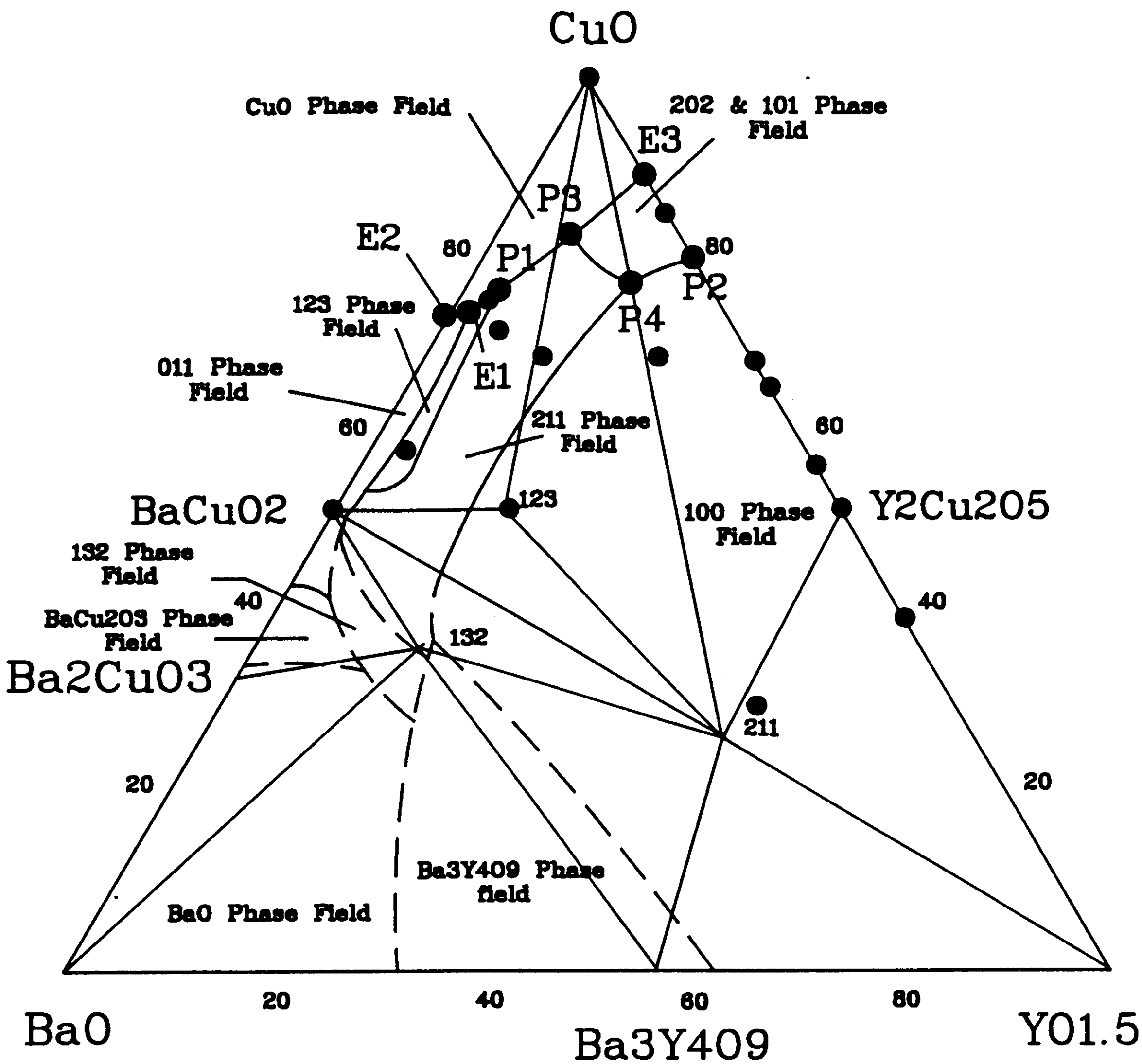

New liquidus phase equilibrium diagram for the $YO_{1.5}$-BaO-CuO ternary system showing eutectic and peritectic reactions determined by this research. Alkemade lines are for compound compatibilities at 950 deg C.

Figure 18.

The following reactions were verified to exist at indicated reaction temperatures:

E1) 123+ CuO + $BaCuO_2$ ==> Liquid 875-890 deg. C

E3) $Y_2Cu_2O_5$ + CuO ==> Liquid 1127-1135 deg. C

E2) $BaCuO_2$ + CuO ==> Liquid 880-930 deg. C

P1) CuO + 123 ==> 211 + Liquid 950-960 deg. C

P2) $Y_2Cu_2O_5$ ==> Liquid + Y_2O_3 1135-1140 deg. C

P3) 211 + CuO ==> $Y_2Cu_2O_5$ + Liquid 950-1080 deg. C

P4) 211 + $Y_2Cu_2O_5$ ==> Y_2O_3 + Liquid < 1080 deg C

General quenched experimental mixture phase compatibilities identified after heating or cooling along a suspected liquidus phase boundary curve were utilized to differentiate between reaction point locations and boundary curve positions. Table 3 list these identified equilibrate phase components with their respective experimental run number, temperature range, and original mixture composition. Phase field relations and areas were also inferred from this information. Phase field areas, boundary curve locations, and ternary reaction points require multiple experimental mixture to locate accurately; therefore only general relationships and approximate location of these entities could be determined from this research data and collect previous studies' data.

TABLE 3.

Summary of Experimental Investigations Completed in the $YO_{1.5}$-Ba-CuO Ternary System

RUN NO.	MOLE PERCENT				TEMP PATH &
	CuO	BaO	$YO_{1.5}$	OBS. PHASES Decreasing Amts	QUENCH TEMP (deg. C)
1.	50.0	33.3	16.7	100	1075
2.	50.0	33.3	16.7	211,011,012	1050
3.	50.0	33.3	16.7	211,011,012	1021
4.	74.2	22.7	3.1	001,012,123,011	925
5.	74.2	22.7	3.1	001,012,123,011	925-890
6.	50.0	33.3	16.7	211,011,012	1020
*7.	50.0	33.3	16.7	123	940-25
*8.	47.5	52.5	0.0	011	880
9.	50.0	0.0	50.0	101,202	1135
10.	74.2	22.7	3.1	012,001	1000
11.	74.2	22.7	3.1	123,012,001,011	1000-708
12.	74.2	22.7	3.1	012,123,001,011	1000-915
13.	59.0	36.0	5.0	123,012,011	980
14.	59.0	36.0	5.0	123,(011),012	980-891
15.	59.0	36.0	5.0	012,123,011	1000
16.	59.0	36.0	5.0	123,011,012	1000-800
17.	68.5	19.5	12.0	012,(001),211	1050-950
18.	68.5	19.5	12.0	012,001,211	1050-930

TABLE 3. CON'T

RUN NO.	MOLE PERCENT CuO	BaO	$YO_{1.5}$	OBS. PHASES Decreasing Amts	TEMP PATH & QUENCH TEMP (deg. C)
*19.	29.0	19.3	51.7	211	1050-1000
*20.	100.0	0.0	0.0	002	1050
*21.	29.0	19.3	51.7	420?	1325
22.	68.5	19.5	12.0	012,202,123,011,001	1080
23.	72.0	22.0	6.0	012,001,211	960
24.	72.0	22.0	6.0	123,001,012,011	960-900
25.	68.6	11.4	20.0	012,202,001	1200
26.	68.5	19.5	12.0	012,202,001	1200
27.	59.0	36.0	5.0	012,001,011	1100
*28.	50.0	0.0	50.0	101 & 202	1125
*29.	67.0	0.0	33.0	101 & 202	1125
30.	67.0	0.0	33.0	101 & 202	1200
31.	55.0	0.0	45.0	101 & 202	1130
32.	55.0	0.0	45.0	101 & 202	1330
33.	65.0	0.0	35.0	101 & 202	1130
34.	65.0	0.0	35.0	101 & 202	1330
35.	85.0	0.0	15.0	101 & 202	1330
*36.	40.0	0.0	60.0	101 & 202 (O_2)	1075
*37.	40.0	0.0	60.0	202 & 101 (O_2)	950

TABLE 3. CON'T

RUN NO.	MOLE PERCENT			OBS. PHASES Decreasing Amts	TEMP PATH & QUENCH TEMP (deg. C)
	CuO	BaO	$YO_{1.5}$		
38.	50.0	0.0	50.0	101 & 202	1135-870
39.	72.0	22.0	6.0	123,012,001,011 (O_2)	950
40.	65.0	0.0	35.0	101 & 202	1200
41.	72.0	22.0	6.0	123,001,012,001	930
*42.	72.0	22.0	6.0	123,011,001	875

* All of these experimental runs had no observed liquid in equilibrated quenched mixtures.

Similar work (5) agrees acceptably with this studies determination of the seven outlined peritectic and eutectic reactions. The eutectic reaction, Liquid ==> 123 + CuO + $BaCuO_2$ at 875-890 degrees Celsius, determined by runs 4, 5, 10, 11, 12, 41, 42, is supported (5). The Binary reaction BaO + CuO ==> $BaCuO_2$ has been determined to exist below 930 deg C and above 880 deg C. Extensive studies in the $YO_{1.5}$-CuO binary system lead to a $Y_2Cu_2O_5$ and $YCuO_2$ ==> $YO_{1.5}$ + CuO incongruent melting reaction temperature comparable to reported values of 1135-1140 degrees Celsius. No work was completed on the yttrium-barium compounds or the ternary 132 compound. Experimental run 21 however, did contain an unknown phase suspected to be BaY_2O_4.

Ternary Reaction Temperatures and Phase field areas

The pseudo-binary A-A′ located along the section line in figure 19 and represented in figure 20 displays experimental control used to develop phase field locations along the ternary section. This diagram is a new psuedo-binary detailing accurate phase equilibrium relationships not previously considered.

Figure 21 is a pseudo-binary B-B′ (see figure 19) detailing quench temperatures and equilibrated phase compo-

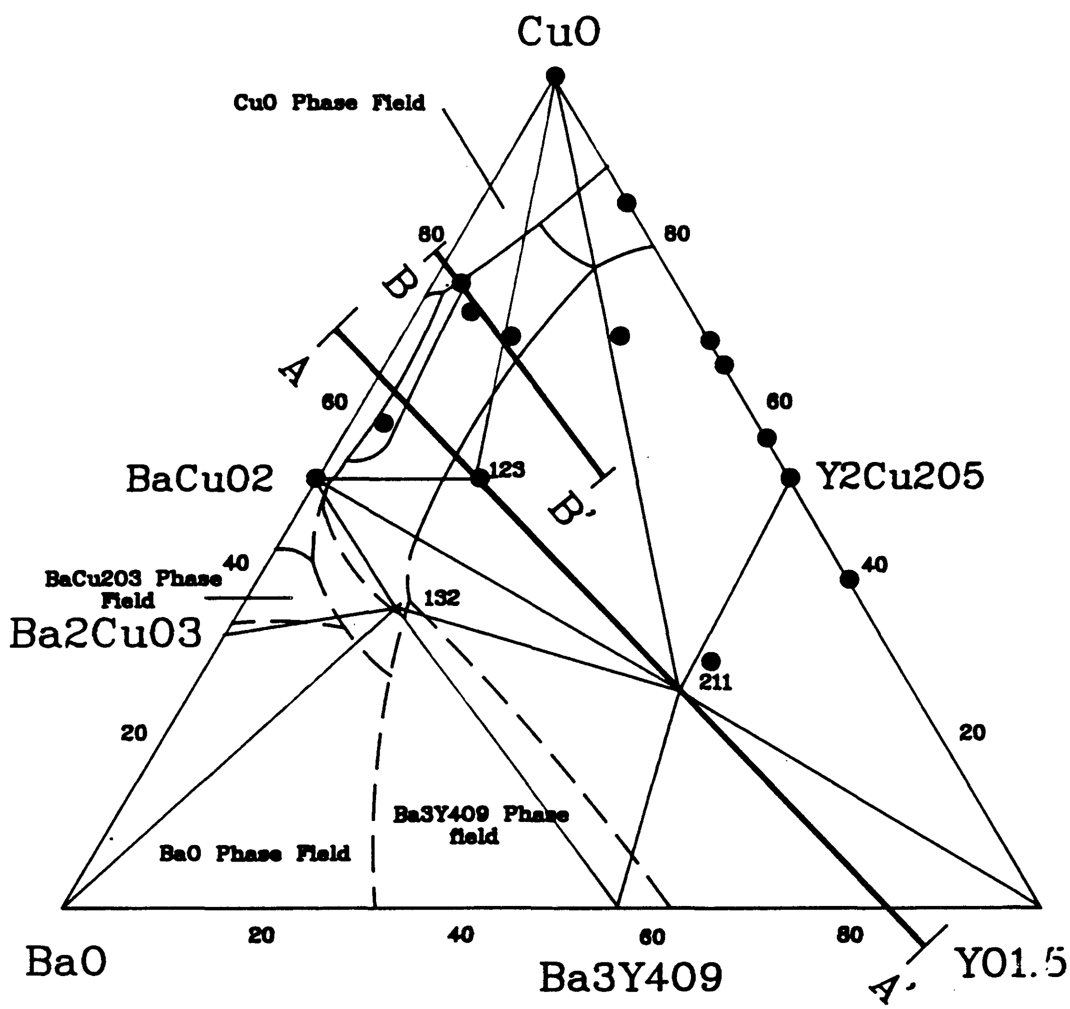

Ternary psuedo-binary section locations. Section A-A' figure 20 and section B-B' figure 21.

Figure 19.

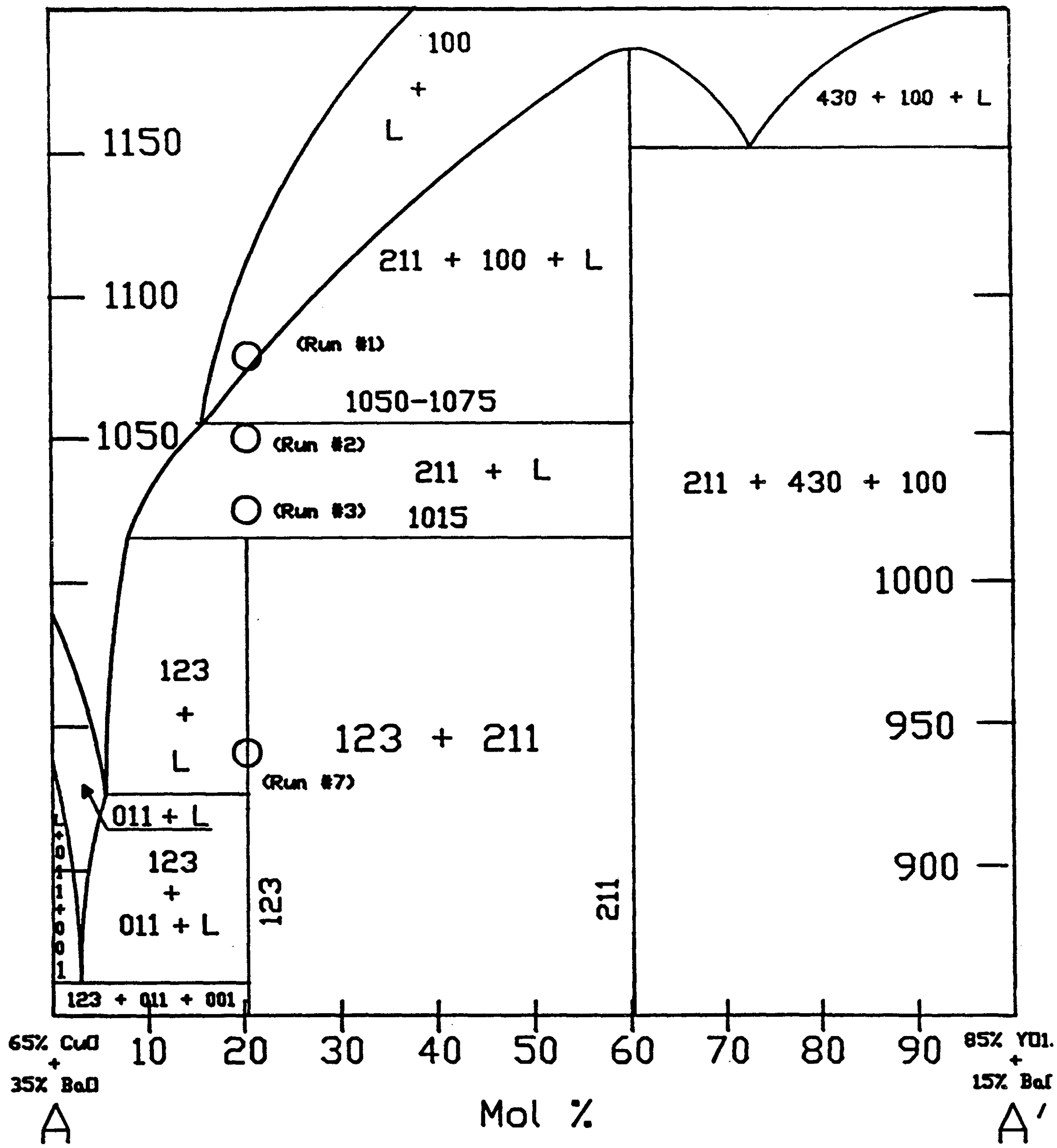

Psuedo-binary section A-A' details 123 phase field relations with $YO_{1.5}$, 211, and $BaCu_2O_2$. Open circles represent experimental control from this study with respective experimental run numbers.

Figure 20.

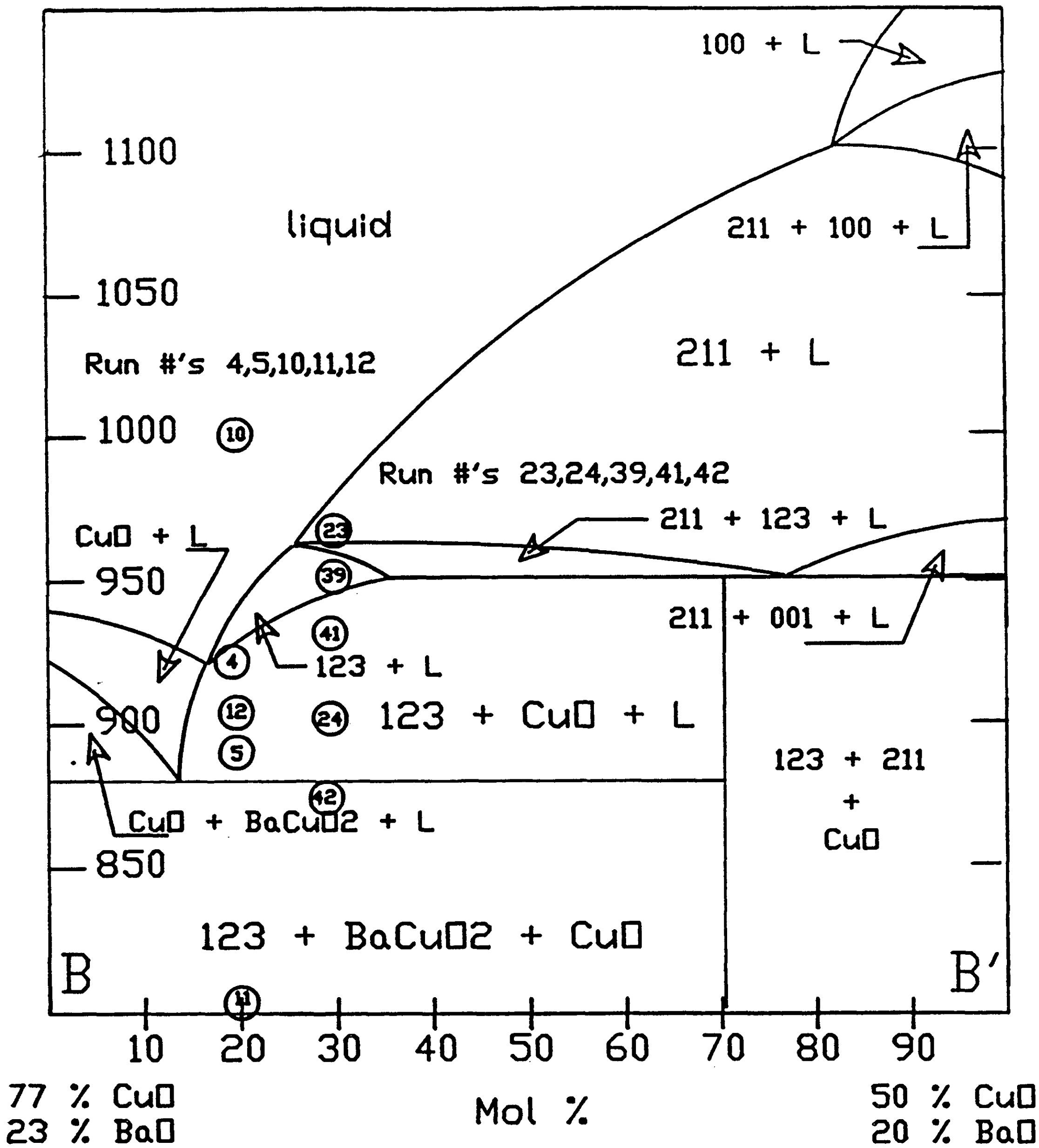

Psuedo-binary section B-B ' details 123 phase field relations with $YO_{1.5}$, 211, CuO and $BaCu_2O_2$ and associated experimental control used to define these relationships. Open circles represent experimental control from this study with respective experimental run numbers.

Figure 21.

nents review and examination for run numbers 4, 5, 10, 11, 12, 23, 24, 39, 41, and 42 which were utilized to isolate 123 + CuO ==> 211 + liquid peritectic reaction temperature and assist with 211, CuO and 123 phase field definition. Each identifiable phase component at a specific temperature fixes that particular component's ternary phase field location with in the diagram. Runs 4, 5, 10, 11, 12, 24, 39, 41, and 42 have no 211 phase present at their respective equilibrated quench temperatures; therefore, this 211 peritectic reaction must occur at temperatures above 925 deg C. Run 23 contains 211; thus, a chemical reaction occurs between run 23's quench temperature of 960 deg C and the highest quench temperature containing no 211 phase at 950 deg. C. Similar arguments can be used to determine additional phase field regions depicted in figure 21 and with other experimental run compositions utilized to define other equilibria relations in the $YO_{1.5}$-BaO-CuO diagram.

Runs 23 and 24 also indicate that the 123-211 reaction boundary curve should be located further towards the BaO-CuO binary. Run number 23 at equilibrium contains 211 as a phase component at 960 deg C. This is explained by positioning the composition point at 960 deg C within the 211 primary phase field. This also relocates the;

211 + liquid ==> CuO + 123

peritectic reaction point, which is intersected by the CuO primary phase boundary curve. Once below the peritectic reaction point temperature of 950-960 deg C the 211 phase should disappear as observed in run 24.

Presence of 202 or 101 in runs 17, 18, 22, 25, 26 instead of the expected and Y_2O_3 primary phase is probably associated with the similar absence of Y_2O_3 in the $CuO-YO_{1.5}$ binary system for compositions cooling in the Y_2O_3 primary field. Yttrium ions in the liquid portion of the melt are more stable when complexed with monovalent copper, so that no free Y_2O_3 is observed in the ternary or binary systems when CuO contents exceed 50 mole percent.

Run No. 22 has five separate phase components some of which are unexpected compatible phase compounds in this area of the system. Equilibrium was probably never achieved in this sample for temperatures recorded in the laboratory. The peritectic reactions:

123 + CuO ==> 211 + Liquid at 940 deg C

and

211 + CuO ==> 202 + L at 975 deg C.

demonstrate possible component relations responsible for the presents of 123 and 011 in run 22.

The experimental final compositions suggest that 132 compatibilities require parent mixtures with greater than 50 mole percent BaO and less than 50 mole percent CuO but, can only be included as equilibrate ternary components if the 132 and associated compounds do not belong to an oxycarbonate compound group.

Multivalent CuO Melts and $BaCu_2O_2$ Formation

Investigations 1-27 all contained an unidentified phase component. This unknown phase was finally identified to be $BaCu_2O_2$. Several $BaCu_2O_2$ experimental run x-ray patterns were averaged obtaining a representative diffraction pattern that was compared to several standard patterns. An excellent match was found between the experimental $BaCu_2O_2$ patterns and a $BaCu_2O_2$ pattern reported by T. Asleage et. al. (12). Similar CuO multivalent system reaction causing $YCuO_2$ formation in the binary system are responsible for $BaCu_2O_2$ existence in the ternary system. Unlike the $YCuO_2$ phase, $BaCu_2O_2$ has been shown to be an unequilibrated system component. Liquid CuO apparently causes lower oxidized phase compound formation i.e. $YCuO_2$ v.s. $Y_2Cu_2O_5$ and $BaCu_2O_2$ v.s. $BaCuO_2$.

During CuO melting it is believed (13, this work) that copper forms an divalent and univalent copper oxide melt ($CuO + Cu_2O$); therefore lower valence state copper atoms exist forming compounds with lower oxygen stoichiometreic ratios then normally expected with a pure CuO melt, subsequently $BaCu_2O_2$ and $YCuO_2$ will form in their respective chemical systems in addition to expected equilibrium phase species when copper liquid is present. System oxygen potential was investigated but, had insignificant effect on relative $BaCuO_2$:$BaCu_2O_2$ ratios that formed when mixtures were heated above eutectic reaction points. To investigate liquid CuO effect on relative $BaCu_2O_2$ and $BaCuO_2$ formation, two mixtures, 41 and 42, were prepared with duplicate compositions but processed with different heating paths. One mixture was heated to hyper-eutectic temperatures, the other mixture remained below eutectic reaction temperatures. Thus, a liquid formed in the first mixture but not in the second. Phase components examination of the two mixtures after quenching revealed that only the melted mixture contained both a $BaCu_2O_2$ phase component and the expected $BaCuO_2$ equilibrated component.

Quenched Liquid Phase components

During quenching, some unexpected phase components appeared frequently in the analyzed mixtures. The phase components were consistently the same compound set or group and relative concentrations were observed to be dependant on liquid phase amounts present at sample quenching. These unequilibrated phase components $BaCu_2O_2$, CuO and sometimes $YCuO_2$ and $BaCuO_2$ represent a quenched liquid phase composition and are demonstrated to be unequilibrated compounds by the following arguments. These phases are compounds which require Cu ions to be both monovalent and divalent. As CuO melts into $Cu^{1+} + Cu^{2+} + (O_2)^{-2}$ ions, melt quenching initiates reaction of these copper-oxide ions with barium and yttrium ions. These reactions progress in the indicated order:

Liquid		Crystalline solids
$Cu^{1+} + Cu^{2+} + O^{-2}$	==>	1) $BaCu_2O_2$
		2) $Y_2Cu_2O_5 + YCuO_2$
		3) $BaCuO_2$
		4) CuO

The barium ions react first with monovalent copper ions, proceeded by yttrium ions, usually present below x-ray detection limits of 1-2%. Most of the yttria reacts next with divalent copper ions, after which remaining barium ions solidify by reaction with divalent copper ions followed by residual divalent copper ions crystalizing to form pure CuO solid. Most monovalent copper ions are extracted by reaction with barium ions, thus residual divalent ions react with remaining barium and yttrium ions in the liquid melt forming normal equilibrated components if monovalent copper reactions have not shifted the initial starting composition out from the original compatibility triangle. The barium ions usually extract most of the monovalent copper ions from the liquid phase leaving only divalent copper ions to react with remaining yttrium and barium ions in the liquid melt. The preferential reaction series phenomena explains Cu_2O absence when liquids above the divalent copper reducing temperature of 1026 degrees Celsius are quenched. No Cu^{1+} ions are available because they have already reacted with liquid component barium and yttrium species.

Cu^{1+} reactivity and $BaCu_2O_2$ and $YCuO_2$ compound stabilities retard system ability to achieve true ternary equilibrium when a multivalent copper-oxide liquid is present. Because CuO melts to a multivalent component liquid an additional parent component Cu_2O is now available to react in the system; therefore the previously designated ternary system is now a quaternary chemical system. Quaternary systems may have four separate phase components present; thus explaining the existence of four phases present in an equilibrated quenched mixture.

Runs 13, 14, and 15 in Table 3. show this liquid quench reaction system explicitly. Run 15 with the highest quench temperature has a corresponding high relative liquid amount present represented by $BaCu_2O_2$ (012) when compared with decreasing relative 012 amounts in continued decreased quench temperatures in runs 14 and 13 respectively. Therefore, mixtures containing greater than three phase components identified, one or more of the previously mentioned compounds ($BaCu_2O_2$, CuO, etc.) that form from a quenched liquid represent a singular liquid phase; thus the phase rule is obeyed for mixtures similar to run number 12 were four separate equilibrium mixture pounds were identified but, the 012, 011 and some 001 actually represent a liquid phase component at quenching indicating, true equilibrated phases at mixture 12 quenching include: Liquid, 123, and 001, agreeing acceptably with the figure 14 diagram. Similar arguments can be used for other run mixtures.

Conclusions

Preliminary objectives to resolve existing discrepancies in literature and to construct a new equilibrium phase compatibility diagram has been achieved. These investigations provide accurate 123 primary phase field area location and delineated adjacent 211, CuO and $BaCuO_2$ phase field boundary and eutectic and peritectic reaction chemistries and temperatures. Comparing work by T. Asleage et. al. (5), which is in reasonable agreement with data from this study provides additional confidence to the newly defined or verified system relations. The new diagram developed from this research has significantly increased confidence and accuracy in the current liquidus phase equilibrium diagram. Further work is required to understand complete relationships along the $BaO-YO_{1.5}$ and BaO-CuO binaries, the phase field relations of these binary systems with ternary 132 and associated compatible compounds, and to determine if these 132 and associated compounds are oxycarbonates. Oxygen potentials in this system appear to have insignificant effects on the equilibrium component ratios when O_2 partial pressures range from 1 atmosphere to less then .2 atmospheres. Segregation of liquidus phase during processing was also determined to be a negligible effect when investigating equilibrium conditions. Importantly existence of more than three phase components in equilibrated mixtures has been explained, by formation of multivalent copper oxide liquid and preferential copper monovalent reaction with liquid barium and yttrium ions, permitting the accurate interpretation of the data.

123 phase relationships at the liquidus surfaces, especially the pseudo-binary shown in figure 15, permitted development of a new processing technique to form pure (less than 1-2 percent impurities), 123 superconducting material.

Chapter VII

Reaction Liquid Forming

Introduction

Development of a new processing technique has allowed 123 superconducting material fabrication from a liquid phase. This new process produced 123 orthorhombic "A" (8) material with measured densities between 95 and 97 percent theoretical. Miessner effect response of these 123 materials indicates that the sample is superconducting. Oxygen stoichiometric optimization equal to 6.5 in the 123 structure has not been attempted. Oxygen transport in the liquid phase during fabrication is sufficient to a permit most of the bulk 123 material to have an oxygen stoichiometric ratio of 7.0; thus some 123 material is not superconducting but this problem can resolved with slight adjustments to the fabrication procedure. This new technique, which allows fabrication of pure materials from a liquid state that normally form incongruent melts resulting in impure phase component contents, is also applicable to other ceramic oxide and composite material chemical systems.

During investigation of the $YO_{1.5}$-CuO binary system, concern that possible segregation of material as a cause of unequilibrated $YCuO_2$ phase composition formation in experimental mixtures was investigated. A simple solution to examine segregation effects of liquid CuO in the mixtures entailed pre-separation of the parent compounds, $YO_{1.5}$ and CuO, into separate layers. Stoichiometric ratios of lower melting temperature CuO was deposited on top of a lightly packed $YO_{1.5}$ layer which has a much higher melting temperature. Subsequently the sample was heated until the CuO formed a reaction liquid and by gravitational and surface tensional forces wetted and infiltrated the $YO_{1.5}$ layer reacting to form relatively pure $YCuO_2$. After careful examination of the reacted products two separate systems were identified:

1) The upper portion of the experimental mixture, previously pure CuO powder had reacted with the lower Y_2O_3 under solid state conditions to form $Y_2Cu_2O_5$.

2) The $YO_{1.5}$ layer was very hard and dense indicating a solidified liquid had reacted to form mostly $YCuO_2$.

The x-ray diffraction patterns of these two systems is shown in figures 15 & 16. Higher oxygen potentials in the upper CuO layer micro system are responsible for $Y_2Cu_2O_5$ formation and lower oxygen potential or diffusion rates in the compacted $YO_{1.5}$ layer resulted in preferential $YCuO_2$ formation.

Application of this technique to 123 fabrication became immediately apparent. Thermodynamic and kinetic process control were considered and an experiment was designed to test the process on a different chemical system (see fig 20) and to fabricate pure 123.

Process Thermodynamic and Kinetic Criteria

Chemical reaction or geometrical change in a system will only occur if a sufficient diving force is present. The general driving force can be define as any system free energy decrease resulting from chemical or mechanical change to the system. However; this change in system free energy must be sufficient to over come any kinetically related barriers which oppose the system tendency to reach a lower free energy state. These thermodynamic and kinetic criteria for the reaction liquid forming process are inferred as follows:

1) In any chemical system for which two or more components are in contact and has reaction kinetics sufficient to allow reactions to occur, a chemical reaction will take place if an intermediate compound exists containing some elements of the parent unequilibrated components.

2) The Young -Dupre equation (14):

$$\gamma_{lv} \bullet \cos\theta = (\gamma_{sv} - \gamma_{sl})$$

provides mechanistic relationships that express the potential for one phase to wet an adjacent phase at an interfacial contact.

3) Assuming that the three components of our system are pure and that vapor phase reaction terms and change in vapor species concentrations can be neglected, tendancy for wetting or reaction spreading of the reaction liquid on the solid can be approximately defined by (15):

$$\gamma_{sl} = g^{sl} - \sum_i \mu_i{}^{sl}\Gamma_i$$

The relation between change in system interfacial surface tensions (γ_{sl}) and a change in free energy associated with chemical reaction is demonstrated in figure 22 and correlates a drop in surface tension associated with an incremental drop in free energy. This initial drop allows wetting or reaction spreading at the reaction interface. As this reaction front migrates, the previously reduced surfaces tensions return towards their original status quo value as chemical equilibrium with this region has again been established.

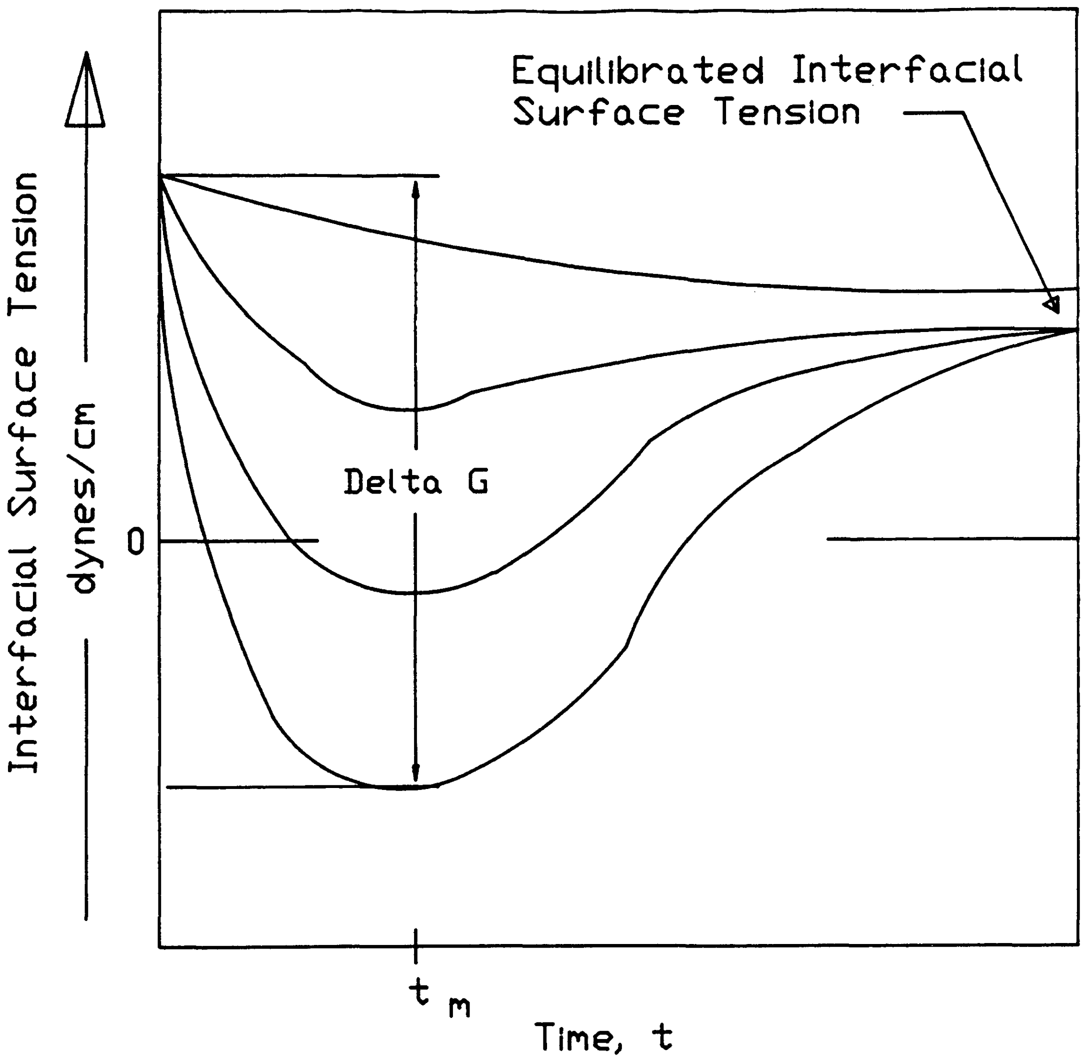

Representation of a drop in interfacial surface tension associated with an incremental decrease in free energy resulting from an interfacial chemical reaction. As the interface returns to chemical equilibrium, after reaction, the surface tension returns to previous status quo values. The top curve represents absorption not reaction of one phase into the other. This decrease in surface tension is responsible for promotion of reaction spreading or wetting of the adjacent phases.

Figure 22.

Once system interfacial wetting or reaction spreading occurs infiltration kinetics (16) will cause the reaction liquid to penetrate the solid substrate, subsequently advancing the reaction interface.

Reaction Liquid Forming Process Technique

This process is designed to allow control of reactions in a binary or psuedo-binary system to permit fabrication of near pure incongruent melting compounds from a liquid melt or permit limitation or preferential reactions through mechanical and chemical constraints. Figure 20 is a Y-Ba-CuO ternary diagram pseudo-binary section along the 123-211 alkemade line and will assist demonstrating the basic principles required for reaction liquid forming of a specified compound. When determining processing reaction criteria it is necessary to work out the logistics on a section diagram or binary system diagram.

1) To Fabricate a pure incongruent melting compound (ICMC) two adjacent compounds are selected ($BaCuO_2$ and 211), each in equilibrium with the specified ICMC (123) and located on opposite sides of the ICMC's composition. These two selected compounds are not in equilibrium along the binary or ternary section line however, they may have a common alkemade line somewhere within the ternary diagram.

2) A precise ICMC (123) stoichiometric mixture made from the two selected non-equilibrated compounds is then prepared. The individual compounds comprising the stoichiometric ratio of 123 compound are not blended.

3) The higher melting temperature compound (211) is then placed in the desired container and may be preformed or compacted if required. Precompaction upto 5 ksi may be necessary to retard reaction kinetics for some systems. Subsequently the lower temperature melting compound ($BaCuO_2$) is placed directly on top of the higher melting compound but, not mixed.

4) The composite mixture is then heated slightly above the lowest eutectic or peritectic reaction temperature (930 C) which contains the ICMC compound.

5) Reaction time will vary depending on reaction kinetics but, optimum heat soak time should not exceed the time required for complete mixture reaction. Quenching of the final material may be necessary to retard continuing reactions.

Conclusion

This technique has effectively reduced inherent melt textured incongruent melting compound impurities by form 10-15% to less than 1-2%, while producing components with 95 or higher percent theoretical densities. Significant advantages in processing are realized including the ability to dope or add special additives into the fabricated material because of increased solubility associated with a reaction liquid present during fabrication. This phenomena was responsible for allowing pure 123 orthorhombic "A" formation which previously could not be formed in sintered material with densities greater than about 85 percent theoretical because of oxygen diffusion restriction into the material.

Cited References

1. J.G. Bednorz and K.A. Muller, Z. Phys B 64 (1986) 189.

2. K.G. Frase and D.R. Clarke, "Phase Compatibilities in the System Y_2O_3-BaO-CuO", Advanced Ceramic Materials, vol. 2, No. 3B, Special issue, pp. 295-302, July 1987.

3. R.S. Roth, K.L. Davis and J.R. Denis, "Phase Equilibria and Crystal Chemistry in the System Ba-Y-Cu-O", Advanced Ceramic Materials, vol. 2, No. 3B, Special issue, pp. 303-312, July 1987.

4. G. Wang, S.J. Hwu, S.N. Song, J.B. Ketterson, L.D. Marks, K.R. Poeppelmieer, and T.O. Mason, "950 Deg C Subsolidus Phase Diagram for Y_2O_3-BaO-CuO System in Air", Advanced Ceramic Materials, vol. 2, No. 3B, Special issue, pp. 313-326, July 1987.

5. T. Asleage and K. Keefer, "Liquidus Relations in the Y-Ba-Cu Oxides", Journal of Material Research, Vol. 3,No. 6. pp. 1279-1291, Nov/Dec 1988.

6. R.S. Roth, C.J. Rawn, F. Beech, J.D. Whitler, J.O. Anderson, "Phase Equilibria in the System Ba-Y-Cu-O-CO_2 in Air", Private Copy, June 1988.

7. Byeong-Joo Lee and Dong Nyung Lee, "Calculation of Phase Diagrams for the $Y_{1.5}$-BaO-CuO_x System", Journal of the American Ceramic Soc., vol. 72, No. 2, pp. 314-319, February 1989.

8. W. Wong-Ng. L.P. Cook, C.K. Chiang, L.J. Swartzendruber, L.H. Bennett, J. Blendell and D. Minor, "Structural Phase Transition Study of $Ba_2YCu_3O_{6+x}$ in Air", Private Copy, July 1988.

9. W. Wong-Ng, H.F. McMurdie, B. Paretzkin, Y. Zhang, K.L. Davis, C.R. Hubbard, A.L. Dragoo, and J.M. Stewart, "X-ray Diffraction Powder Patterns of Sixteen Ceramic Phases", Private Copy, June 1988.

10. D.M. Deleeuw, C.A.H.A. Mutsafers, C. Langereis, H.C.A. Smoorenburg and P.J. Rommers, "Compounds and Phase Compatibilities in the System Y_2O_3-BaO-CuO at 950 Deg C", Physica C, vol. 152., pp. 39-49, Jan 1988.

11. *Phase Diagrams for Ceramists*, vol. I-IV., Edited and Published by: The American Ceramic Soc. Inc., 1965-1981, Figures: 209, 2105, 2297, 2299, 5178, 5132, 5129.

12. *JCPDSF - Inorganic Hanawalt Search Manual*, 1983.

13. T. Aselage, Private Communication, April 1989.

14. I.A. Askay, C.E. Hoge, and J.A. Pask, " Wetting Under Chemical Equilibrium and Nonequilibrium Conditions", Journal of Physical Chemistry, vol. 78, No. 12, pp. 1178-1183, 1974.

15. Joseph A. Pask, " From Technology to the Science of Glass/Metal and Ceramic/Metal Sealing", Ceramic Bull., vol. 66, No. 11 pp. 1587-1592, 1987.

16. G.P. Martins, D.L. Olson, and G.R. Edwards, " Modeling of infiltration Kinetics for Liquid Metal Processing of Composites", Metallurgical Trans. B, vol. 19B, pp. 95-101, February 1988.

APPENDIX A

HEATING & COOLING PATH DIAGRAMS

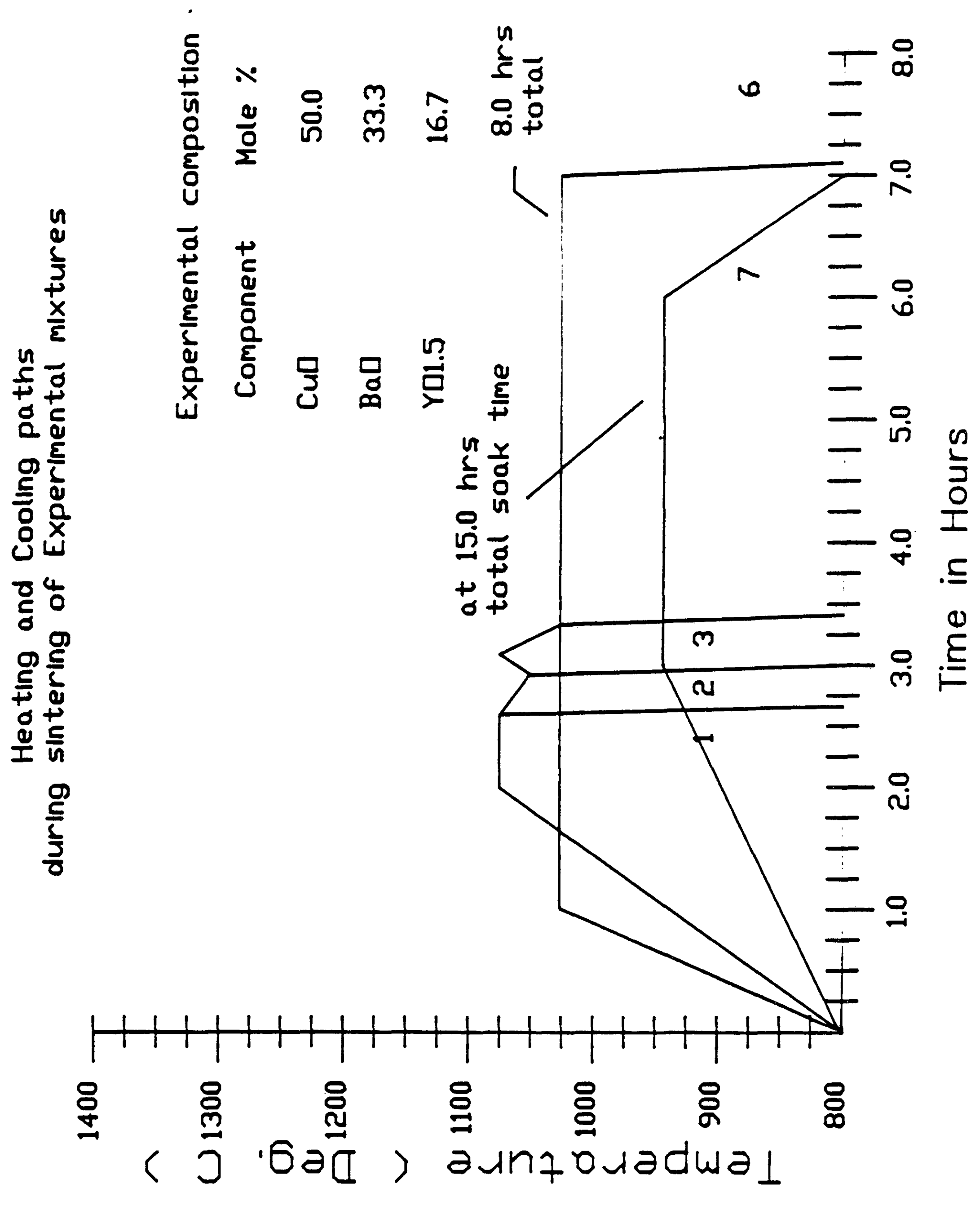

Heating and Cooling paths
during sintering of Experimental mixtures
Experimental composition
Component Mole %
CuO 50.0
BaO 33.3
YO1.5 16.7
at 15.0 hrs
total soak time
8.0 hrs
total
1
2
3
6
7
Temperature (Deg. C)
1400
1300
1200
1100
1000
900
800
1.0
2.0
3.0
4.0
5.0
6.0
7.0
8.0
Time in Hours

Figure A - 1

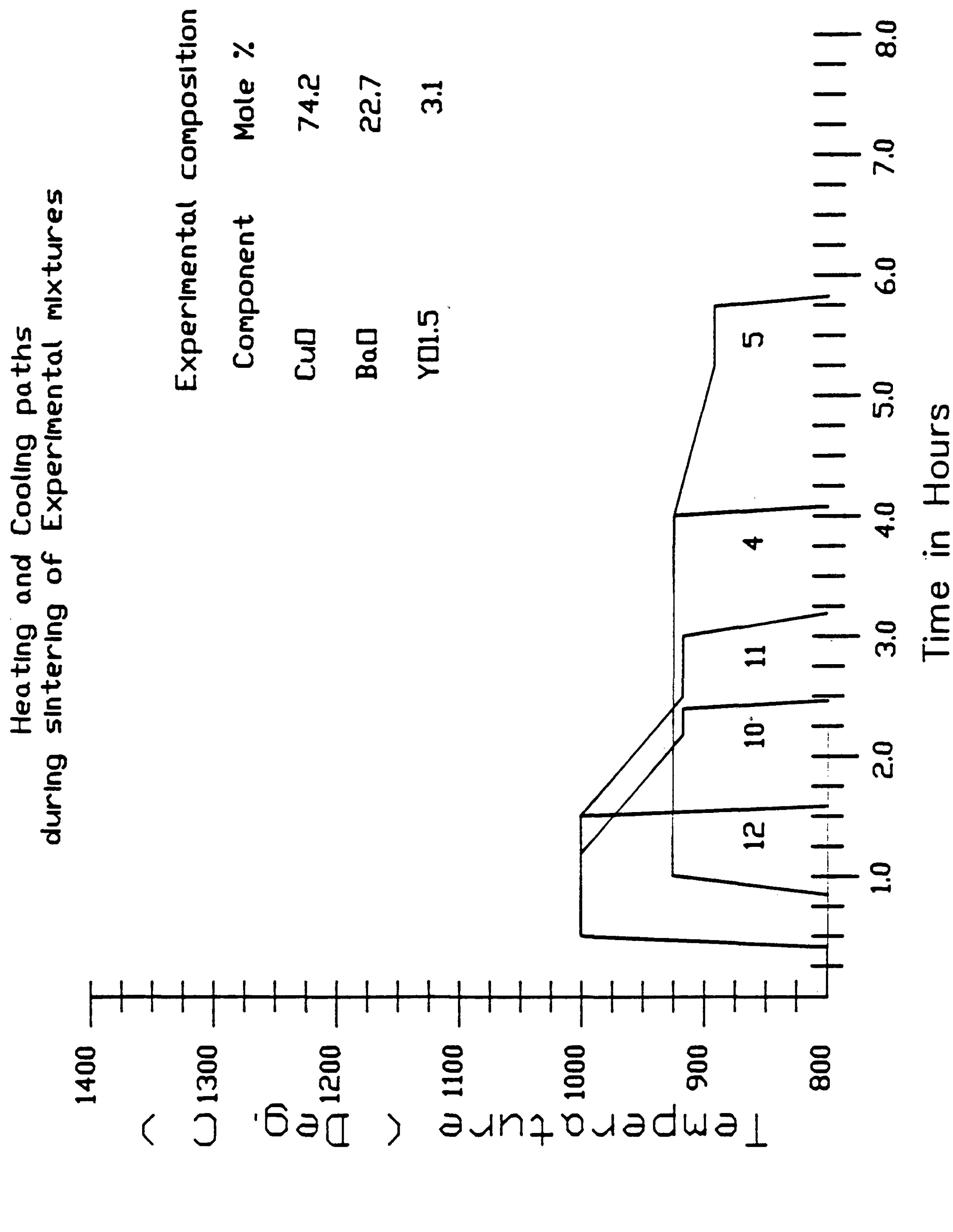
Heating and Cooling paths
during sintering of Experimental mixtures
Experimental composition
Component
Mole %
CuO
74.2
BaO
22.7
YO1.5
3.1
12
10
11
4
5
Temperature (Deg. C)
1400
1300
1200
1100
1000
900
800
1.0
2.0
3.0
4.0
5.0
6.0
7.0
8.0
Time in Hours

Figure A - 2

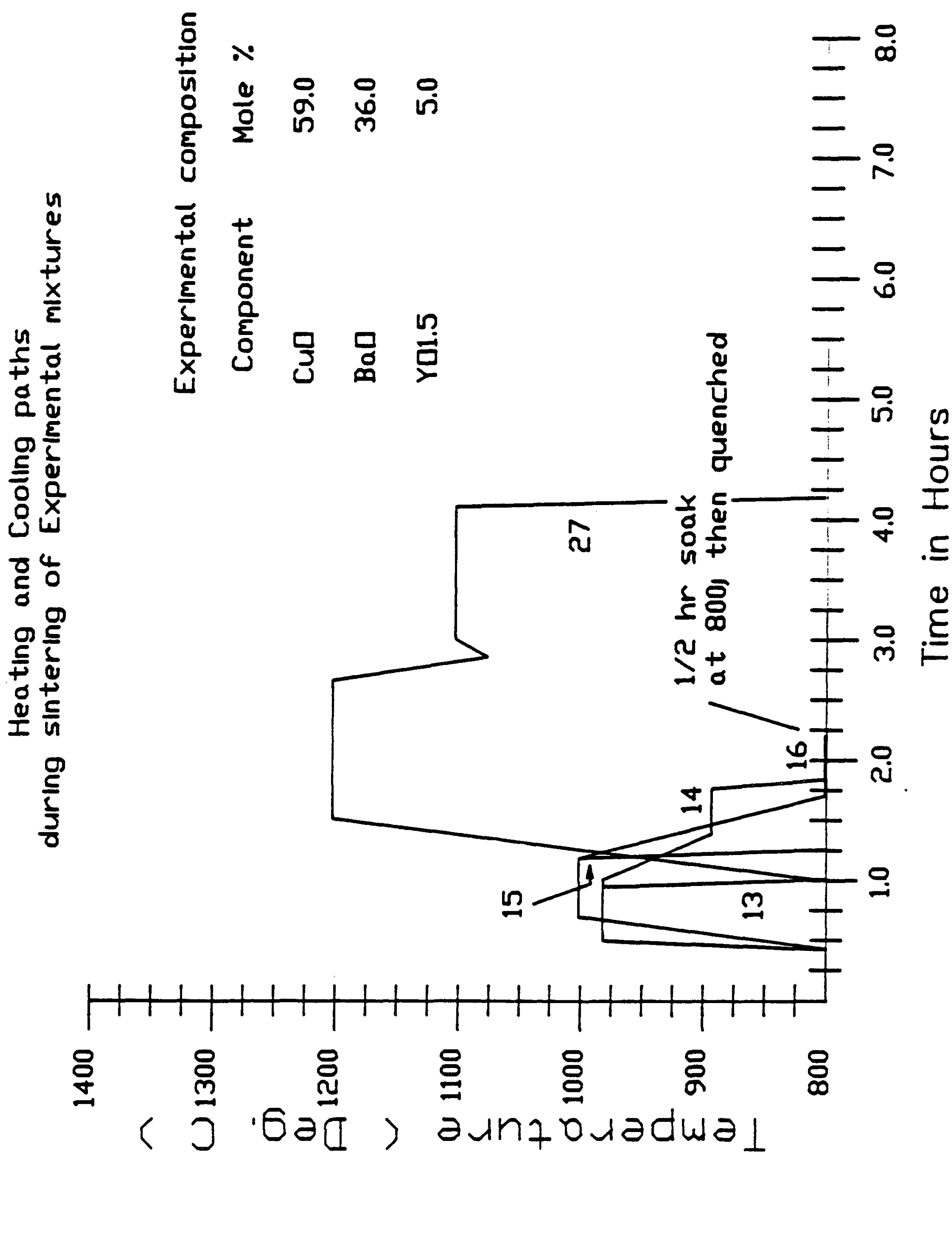
Heating and Cooling paths
during sintering of Experimental mixtures
Experimental composition
Component
Mole %
CuO
59.0
BaO
36.0
YO1.5
5.0
1/2 hr soak
at 800, then quenched
27
16
14
15
13
Temperature (Deg. C)
1400
1300
1200
1100
1000
900
800
1.0
2.0
3.0
4.0
5.0
6.0
7.0
8.0
Time in Hours

Figure A - 3

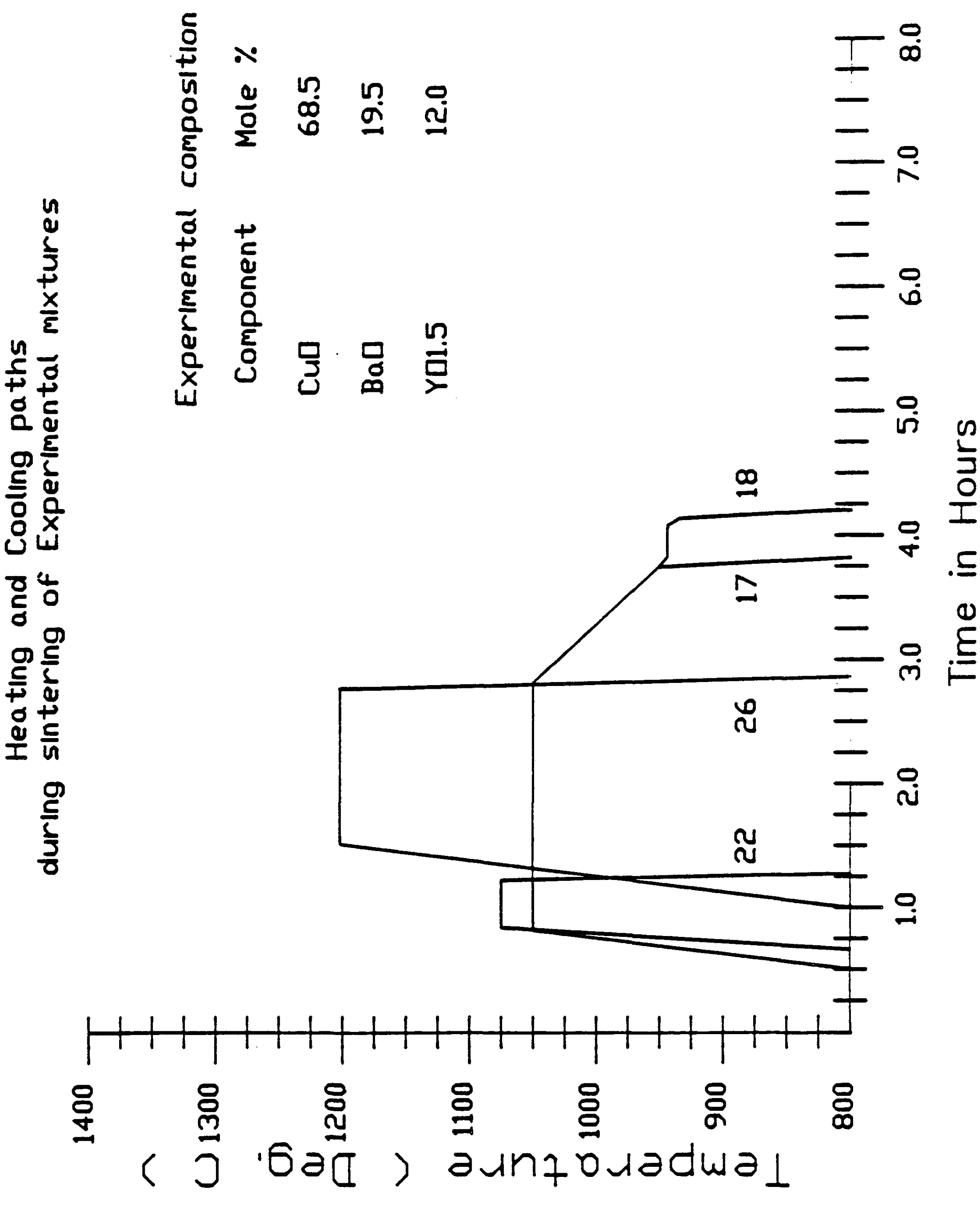
Heating and Cooling paths
during sintering of Experimental mixtures
Experimental composition
Component
Mole %
CuO
68.5
BaO
19.5
YO1.5
12.0
22
26
17
18
Temperature (Deg. C)
1400
1300
1200
1100
1000
900
800
1.0
2.0
3.0
4.0
5.0
6.0
7.0
8.0
Time in Hours

Figure A - 4

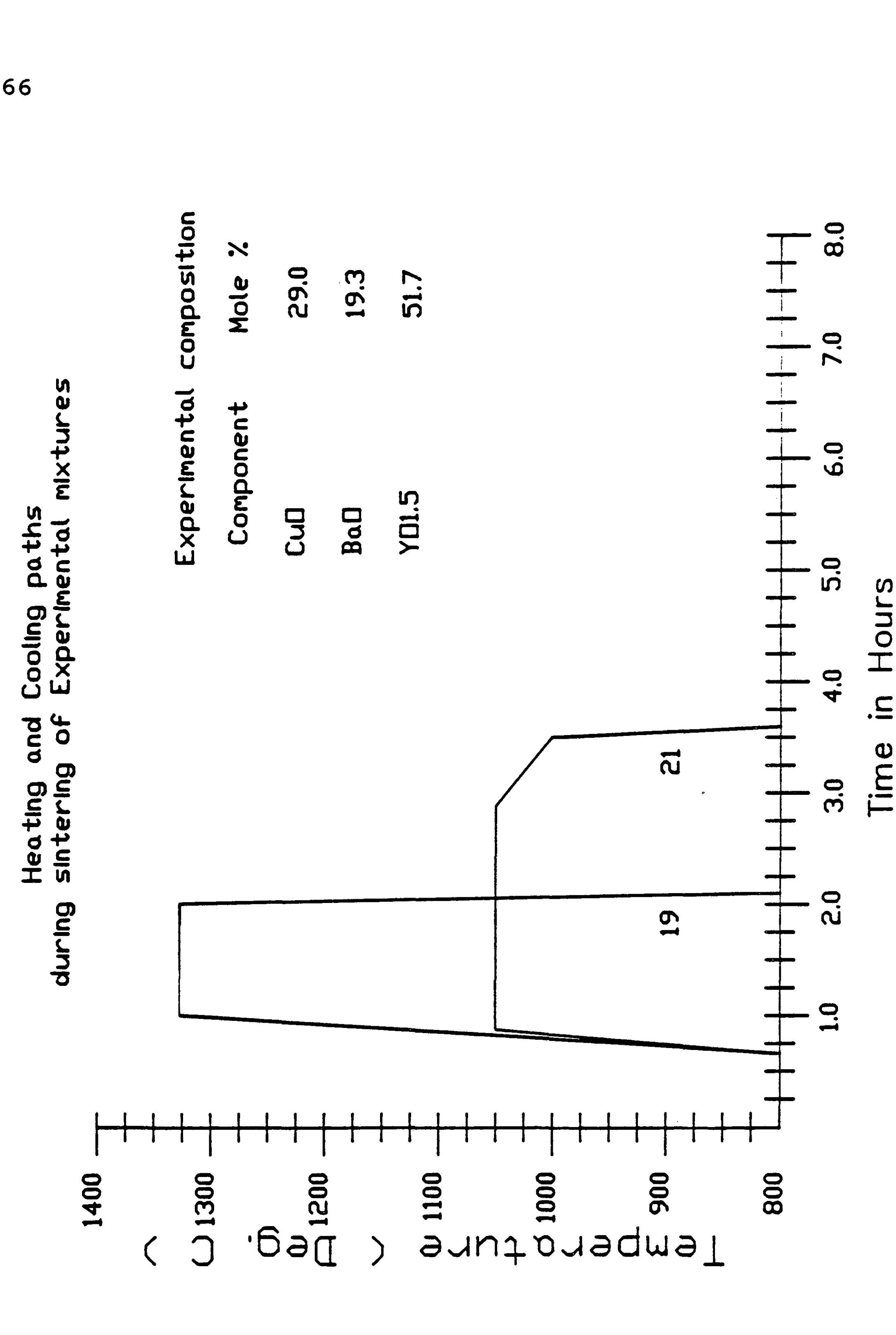
Heating and Cooling paths
during sintering of Experimental mixtures
Experimental composition
Component Mole %
CuO 29.0
BaO 19.3
YO1.5 51.7
19
21
Temperature (Deg. C)
1400
1300
1200
1100
1000
900
800
1.0
2.0
3.0
4.0
5.0
6.0
7.0
8.0
Time in Hours

Figure A - 5

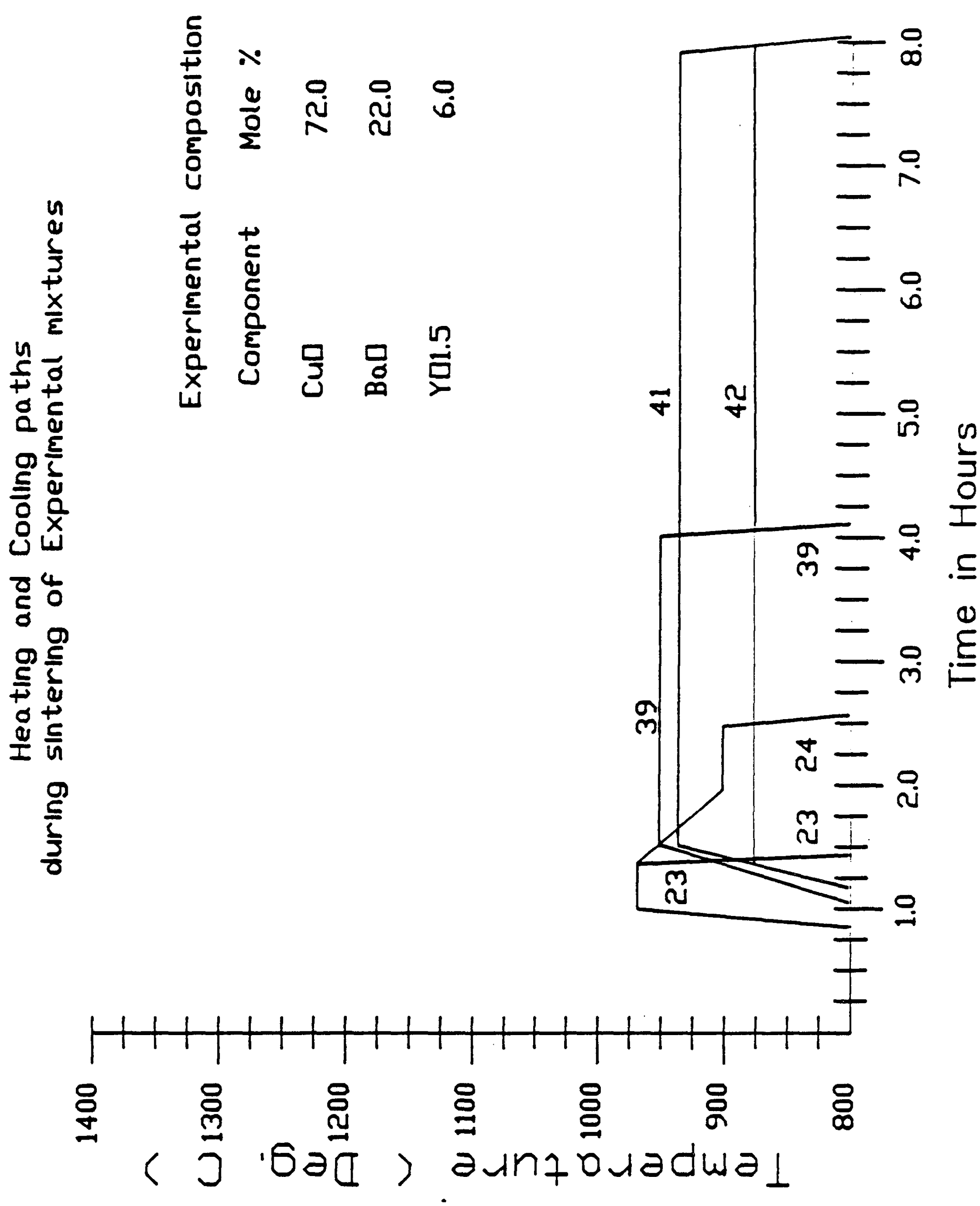
Heating and Cooling paths
during sintering of Experimental mixtures
Experimental composition
Component Mole %
CuO 72.0
BaO 22.0
YO1.5 6.0
23
23
24
39
39
41
42
Temperature (Deg. C)
1400
1300
1200
1100
1000
900
800
1.0
2.0
3.0
4.0
5.0
6.0
7.0
8.0
Time in Hours

Figure A - 6

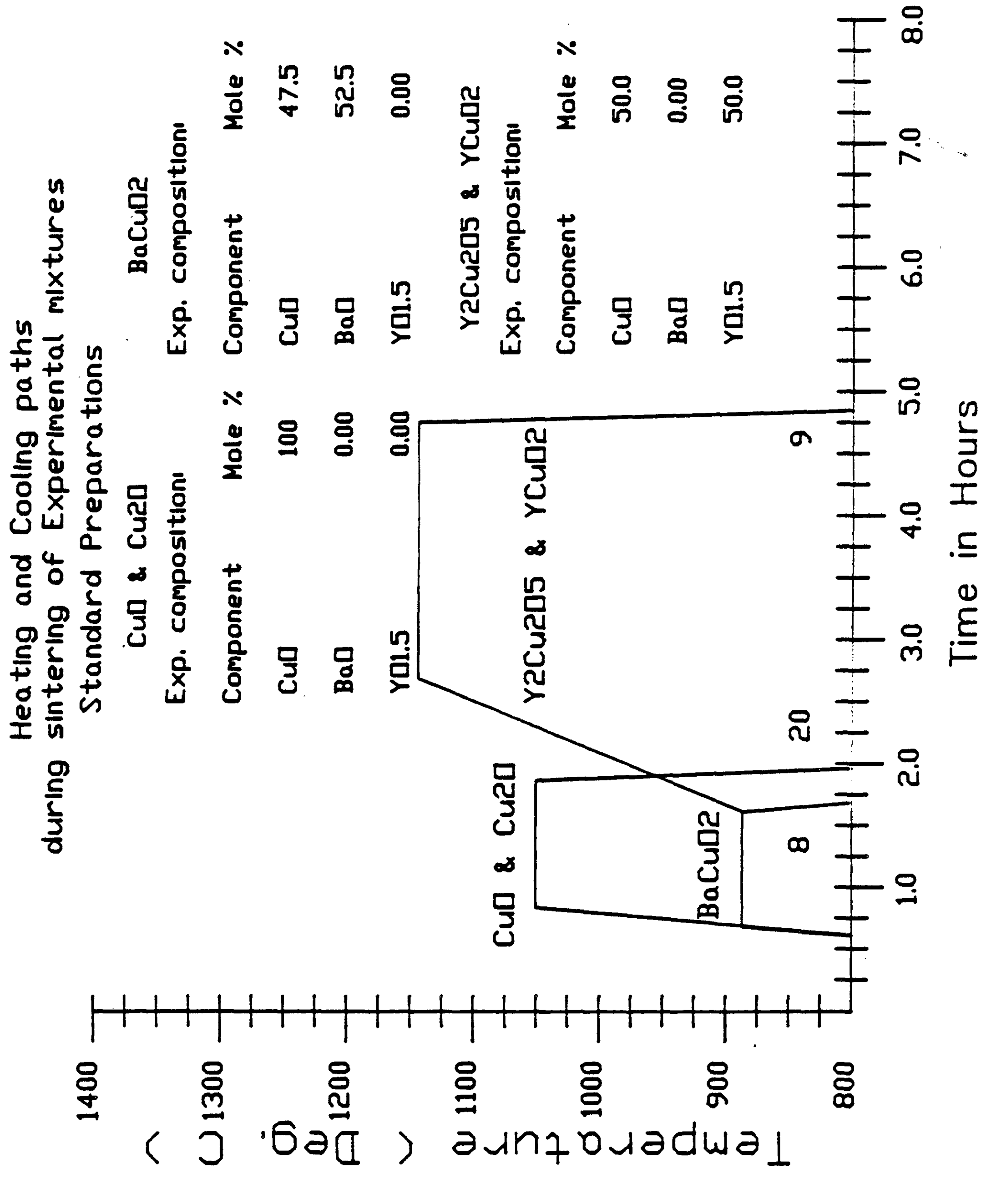

Heating and Cooling paths
during sintering of Experimental mixtures
Standard Preparations
CuO & Cu2O
Exp. composition:
Component Mole %
CuO 100
BaO 0.00
YO1.5 0.00
BaCuO2
Exp. composition:
Component Mole %
CuO 47.5
BaO 52.5
YO1.5 0.00
Y2Cu2O5 & YCuO2
Exp. composition:
Component Mole %
CuO 50.0
BaO 0.00
YO1.5 50.0
CuO & Cu2O
BaCuO2
Y2Cu2O5 & YCuO2
8
20
9
Temperature (Deg. C)
1400
1300
1200
1100
1000
900
800
1.0
2.0
3.0
4.0
5.0
6.0
7.0
8.0
Time in Hours

Figure A - 7

APPENDIX B

RELATIVE X-RAY INTENSITY PATTERNS

RELATIVE INTENSITY DATA
for: CuO

Scan at 40 KV & 25 ma with Cu_K alpha x-rays (1.541838)

LINE No.	d-SPACING (A)	2 THETA(deg)	RELATIVE INTENSITY
1.00	2.75	32.51	7.52
2.00	2.53	35.49	87.77
3.00	2.47	36.38	6.09
4.00	2.33	38.65	100.00
5.00	2.14	42.29	1.99
6.00	1.96	46.22	1.79
7.00	1.87	48.61	31.07
8.00	1.78	51.30	1.77
9.00	1.72	53.41	9.67
10.00	1.59	58.16	14.41
11.00	1.51	61.42	26.61
12.00	1.42	65.69	2.97

RELATIVE INTENSITY DATA
for: Cu_2O

Scan at 40 KV & 25 ma with $Cu_{K\ alpha}$ x-rays (1.541838)

LINE No.	d-SPACING (A)	2 THETA(deg)	RELATIVE INTENSITY
1.00	2.98	29.98	2.85
2.00	2.23	40.48	100.00
3.00	2.05	44.15	3.37
4.00	1.84	49.57	32.94

RELATIVE INTENSITY DATA for: $BaCuO_2$

Scan at 40 KV & 25 ma with Cu_K alpha x-rays (1.541838)

LINE No.	d-SPACING (A)	2 THETA(deg)	RELATIVE INTENSITY
1.00	3.56	25.00	6.37
2.00	3.42	26.09	7.12
3.00	3.33	26.79	13.66
4.00	3.23	27.58	8.94
5.00	3.16	28.24	85.93
6.00	3.11	28.74	19.87
7.00	3.05	29.31	100.00
8.00	2.97	30.13	52.81
9.00	2.89	30.93	18.46
10.00	2.86	31.31	23.01
11.00	2.83	31.66	14.82
12.00	2.64	33.92	40.73
13.00	2.51	35.77	23.10
14.00	2.42	37.11	8.77
15.00	2.33	38.70	15.98
16.00	2.29	39.41	13.82
17.00	2.25	40.09	23.76
18.00	2.16	41.76	30.63
19.00	2.15	42.11	30.46
20.00	2.07	43.73	8.44
21.00	2.04	44.31	7.04
22.00	1.99	45.52	5.63
23.00	1.98	45.87	9.93
24.00	1.96	46.35	9.19
25.00	1.93	47.16	15.65
26.00	1.85	49.27	31.04
27.00	1.81	50.29	10.60
28.00	1.77	51.49	40.81
29.00	1.71	53.65	18.13
30.00	1.69	54.44	10.43
31.00	1.63	56.36	9.11
32.00	1.61	57.40	10.35
33.00	1.58	58.31	20.12

RELATIVE INTENSITY DATA
for: $Y_2Cu_2O_5$ & $YCuO_2$

Scan at 40 KV & 25 ma with Cu_K alpha x-rays (1.541838)

LINE No.	d-SPACING (A)	2 THETA(deg)	RELATIVE INTENSITY
1.00	4.97	17.86	1.22
2.00	4.34	20.48	3.80
3.00	4.08	21.76	3.33
4.00	3.29	27.09	4.89
5.00	3.06	29.15	39.54
6.00	2.94	30.45	5.37
7.00	2.86	31.26	19.09
8.00	2.70	33.20	18.82
9.00	2.68	33.49	11.01
10.00	2.65	33.84	11.96
11.00	2.53	35.54	3.33
12.00	2.50	35.96	2.99
13.00	2.47	36.45	7.61
14.00	2.39	37.57	2.04
15.00	2.32	38.77	4.01
16.00	2.26	39.91	5.98
17.00	2.13	42.38	5.77
18.00	2.08	43.56	6.25
19.00	2.03	44.74	8.90
20.00	1.94	46.94	5.16
21.00	1.90	47.82	7.74
22.00	1.87	48.56	26.22
23.00	1.83	49.80	1.22
24.00	1.82	50.14	1.77
25.00	1.77	51.80	5.71
26.00	1.75	52.33	4.01
27.00	1.72	53.23	3.74
28.00	1.65	55.65	4.48
29.00	1.64	56.24	2.79
30.00	1.60	57.52	22.55
31.00	1.59	58.19	3.40
32.00	1.56	59.04	4.62
33.00	1.56	59.24	3.94
34.00	1.53	60.49	3.40
35.00	1.52	60.81	7.27
36.00	1.51	61.45	3.12
37.00	1.47	63.40	3.33
38.00	1.44	64.60	2.31
39.00	1.42	65.91	2.31
40.00	1.38	68.07	100.00

RELATIVE INTENSITY DATA
for: Y_2BaCuO_5

Scan at 40 KV & 25 ma with $Cu_{K\ alpha}$ x-rays (1.541838)

LINE No.	d-SPACING (A)	2 THETA(deg)	RELATIVE INTENSITY
1.00	3.42	26.06	6.10
2.00	3.06	29.21	18.66
3.00	3.00	29.78	100.00
4.00	2.93	30.53	72.10
5.00	2.83	31.57	45.49
6.00	2.80	31.98	19.35
7.00	2.70	33.14	27.13
8.00	2.65	33.88	5.12
9.00	2.57	34.96	4.73
10.00	2.51	35.81	14.83
11.00	2.42	37.11	13.84
12.00	2.33	38.64	5.42
13.00	2.30	39.14	15.31
14.00	2.21	40.78	30.87
15.00	2.18	41.36	14.32
16.00	2.15	41.96	7.52
17.00	2.07	43.64	14.70
18.00	2.03	44.75	12.60
19.00	1.99	45.61	50.56
20.00	1.94	46.75	11.48
21.00	1.90	48.01	5.98
22.00	1.87	48.72	23.43
23.00	1.78	51.20	19.43
24.00	1.76	51.88	14.57
25.00	1.74	52.57	31.08
26.00	1.68	54.53	11.78
27.00	1.66	55.39	27.09
28.00	1.65	55.82	26.53
29.00	1.62	56.99	7.44
30.00	1.60	57.45	8.04
31.00	1.60	57.77	10.45
32.00	1.56	59.27	28.03
33.00	1.54	60.10	6.71
34.00	1.52	61.02	4.69
35.00	1.50	61.66	20.25
36.00	1.49	62.17	18.96
37.00	1.48	62.72	13.11
38.00	1.46	63.57	10.40
39.00	1.43	65.04	12.08

APPENIDX C

CHEMICAL ELEMENTAL ANALYSIS ON THE PARENT COMPOUNDS $Ba(OH)_2 \cdot 8H_2O$, CuO and Y_2O_3

YTTRIUM OXIDE

Supplied by Molycorp, Inc

Y_2O_3/REO 99.99% min

Specification

CeO_2	< 10	ppm
Nd_2O_3	< 10	"
Pr_6O_{11}	< 1	"
Sm_2O_3	< 1	"
Eu_2O_3	< 1	"
Gd_2O_3	< 10	"
Tb_4O_7	< 1	"
Dy_2O_3	< 1	"
Ho_2O_3	< 1	"
Er_2O_3	< 1	"
Tm_2O_3	< 1	"
Yb_2O_3	< 1	"
CaO	10	"
Fe_2O_3	10	"
SiO_2	5	"
V_2O_5	-	

BARIUM HYDROXIDE

Supplied by Barium and Chemicals, Inc.

$Ba(OH)_2 \cdot 8H_2O$ 98.0% min

Specification

$BaCO_3$	< 2.0%
Insol. HCL	< 0.010%
Cl	< 0.001%
S	< 0.001%
Substance Not ppt in H_2SO_4	< 0.20%
Ca	< 0.05%
Hvy Metals as Pb	< 0.0005%
Fe	< 0.001%
Sr	< 0.8%

COPPER OXIDE

Supplied by Ceramic Color & Chemical MFG. CO.

Specification

CuO	99.80 %
Total copper	80.00 %
Fe	0.02 %
Mg	0.10 %
Cr	0.05 %
Zn	0.20 %
Al	0.10 %
Acid Insols	0.30 %